# Lung macrophages mediate helminth resistance through differential activation of recruited monocyte-derived alveolar macrophages and arginine depletion

Fei Chen[1,2], Darine W. El-Naccache[1,2,3], John J. Ponessa[1,2,3], Alexander Lemenze[1,4], Vanessa Espinosa[1,5], Wenhui Wu[1,2], Katherine Lothstein[1,2], Linhua Jin[1,2], Olivia Antao[1,2], Jason S. Weinstein[1,2], Payal Damani-Yokota[6], Kamal Khanna[6,7,], Peter Murray[8], Amariliz Rivera[1,5], Mark C. Siracusa[1,2,6], and William C. Gause[1,2,6]

[1]Center for Immunity and Inflammation, [2]Department of Medicine, [4]Department of Pathology, Immunology, and Laboratory Medicine, and [5]Department of Pediatrics, New Jersey Medical School, Rutgers—The State University of New Jersey, Newark, New Jersey, USA. [6]Department of Microbiology, New York University Langone Health, New York, NY 10016, USA.[7]Perlmutter Cancer Center, New York University Langone Health, New York, NY 10016, USA,[8] Max Planck Institute of Biochemistry, Martinsried 82152, Germany.

[3]Authors contributed equally
[6]Authors contributed equally

Running title: mechanisms of macrophage-mediated helminth resistance

**Abstract:**

Macrophages are known to mediate anti-helminth responses, but it remains uncertain which subsets are involved or how macrophages actually kill helminths. Here we show rapid monocyte recruitment to the lung after infection with the nematode parasite, *Nippostrongylus brasiliensis*. In this inflamed tissue microenvironment these monocytes differentiate into an alveolar-like macrophage (AM) phenotype, expressing both Siglec-F and CD11c, surround invading parasitic larvae and preferentially kill parasites in vitro. Monocyte-derived AMs (Mo-AMs) express type 2-associated markers and show distinct remodeling of the chromatin landscape relative to tissue-derived AMs. In particular, they express high amounts of Arg1 (arginase-1), which we demonstrate mediates helminth killing through L-arginine depletion. These studies indicate that recruited monocytes are selectively programmed in the pulmonary environment to express AM markers and an anti-helminth phenotype.

82 **Introduction:**

83 Helminth infections trigger potent type 2 immune responses characterized by
84 elevations in IL-4, IL-5, and IL-13. This response mediates host protection through limiting
85 parasite burden and by mitigating tissue damage associated with the trafficking of these
86 large multicellular parasites through host tissues[1]. Although helminth infections represent
87 a major global health problem, effective vaccine strategies remain elusive, likely in part
88 because the cellular and molecular mechanisms through which the anti-helminth
89 immunity is mediated remain unclear. A critical stage of the life cycle of many helminths,
90 including intestinal nematode parasites, involves transit through the host lung. Previous
91 studies have indicated that the lung plays a significant role in early parasite clearance
92 and as such is a potential target for therapeutic and vaccine-strategies to promote host
93 resistance [2,3].

94 Both lymphoid and myeloid cells play important roles in promoting type 2
95 inflammation and anti-helminth immunity. For example, T cells, B cells, myeloid cells and
96 innate lymphoid type 2 cells are activated and promote robust levels of IL-4, IL-5 and IL-
97 13 following a helminth challenge. Importantly, studies also indicate that macrophages
98 and neutrophils contribute to host protection by directly killing parasitic larvae and
99 initiating the healing of parasite affected tissues[3-6]. Neutrophils not only directly target
100 helminths[4], but also stimulate macrophages to assume an alternatively activated state
101 required for their anti-helminth effector functions[3,7]. Recent studies indicate that
102 macrophages primed by helminths in the intestine, lung and skin can mediate helminth
103 killing both in vitro and in these tissue microenvironments[2,3,8-11].

104 Tissue-resident macrophage populations can be subdivided into tissue-derived
105 macrophages (TD-macs) and monocyte-derived macrophages (Mo-macs). TD-macs
106 develop during the early stages of fetal development from the yolk sac and fetal liver, and
107 populate tissues under steady-state conditions, whereas Mo-macs develop from bone
108 marrow-resident precursor cells and can enter tissues in the context of inflammation[12-15].
109 In the lung microenvironment, tissue-derived alveolar macrophages (TD-AMs) mediate
110 homeostasis through multiple mechanisms, including surfactant recycling, and also
111 provide surveillance for early recognition of pathogens invading the airways[16]. Other
112 scarce tissue-derived interstitial macrophage populations also can have distinct
113 properties[17]. During infection monocytes are rapidly recruited to the lung, where they can
114 differentiate into macrophages. Recent studies suggest that monocytes can also
115 differentiate into an alveolar macrophage-like phenotype and that these Mo-AMs can
116 function differently than TD-AMs[18]. In one study, the Mo-AMs were the predominate lung
117 macrophage subset contributing to fibrosis in a bleomycin-induced lung injury model[19].
118 Despite these substantial advances in understanding macrophage ontogeny, studies
119 examining the development of Mo-AMs have primarily relied on radiation chimeras or
120 other non-physiological approaches raising questions as to the physiological significance
121 of these observations. Further, whether Mo-AMs populate the lung and perform distinct
122 functions in the context of helminth infections remains to be determined.

123 Although the anti-helminth qualities of macrophages are well-documented, there
124 is a substantial knowledge gap regarding the mechanisms they employ to promote
125 parasite killing. Previous studies have shown that Arginase (Arg) activity[3,8,20], specifically
126 Arg 1[11], is required for the anti-helminth properties of macrophages. Arg1 is known to

127 mediate a cascade of effects leading to potentially toxic urea production and also
128 polyamine synthesis which may contribute to immune cell activation and proliferation[20].
129 Arg1 can also mediate the localized depletion of arginine, which can have
130 immunoregulatory effects on activated immune cells such as T cells[21]. However, whether
131 any of these or other potentially associated mechanisms are important in mediating
132 macrophage killing of helminth parasites and whether they are distinctly initiated in
133 specific subsets of macrophages remains uncertain.

134 Infection with the intestinal nematode parasite, *N. brasiliensis* (Nb) is a well-
135 established rodent experimental model showing a similar life cycle to human hookworms.
136 Use of this model has substantially advanced our understanding of inflammation and
137 macrophage biology in lung damage and repair caused by transiting helminths. When
138 infected with Nb, infective third-stage larvae (L3) migrate from the skin to the lung before
139 entering the small intestine. In the lung, both innate and adaptive components of the type
140 2 immune response interact with the migrating parasitic larvae[2,5,6]. Previous studies have
141 shown that CD4 T cell depletion at the time of secondary inoculation does not affect
142 accelerated resistance, which is also intact in B cell deficient mice[22,23]. However, lung
143 macrophages primed by primary Nb inoculation have previously been shown to play an
144 important role in acquired resistance and highly purified helminth-primed lung
145 macrophages can effectively kill L3 in vitro[3].

146 Here we investigated the role of lung macrophage subsets of different progenitor
147 origins in mediating acquired resistance to Nb. We further elucidate the role of neutrophils
148 in driving their effector function and reveal how macrophages mediate resistance against
149 helminths via Arg1-dependent mechanisms.

150 **Results:**

151 Nb L3 enter the lung as early as 12 hours after subcutaneous inoculation. To
152 examine how parasite migration through the lung affected numbers of monocytes and
153 macrophages, these populations were analyzed via flow cytometric analysis on days 1,
154 7, and 14 after inoculation. Marked increases in the total number of macrophages
155 (F4/80$^{+}$, CD64$^{+}$) were observed by day 7 after inoculation (**Fig. 1a**) while monocytes
156 (F4/80$^{+,}$ Ly6C$^{+}$) were markedly increased within 24 hours, consistent with their rapid
157 recruitment, peaked at day 7, and had dropped markedly by day 14 (**Fig. 1b**). Alveolar
158 macrophages (AMs) (CD64$^{+}$,F4/80$^{+}$,SiglecF$^{+}$, CD11c$^{+}$) were slightly elevated as early as
159 day 1 but showed marked increases, more than doubling by day 7 (**Fig. 1c**). Non alveolar
160 macrophages (hereafter, referred to as NAMs) (CD64$^{+}$, F4/80$^{+}$, Siglec-F$^{-}$, CD11c$^{var}$), were
161 also markedly elevated by day 7 after Nb inoculation (**Fig. 1d**). In comparison,
162 eosinophils, also associated with Nb infection, were not elevated until day 7 after
163 inoculation and remained elevated at day 14 (**Fig. 1e**). Collectively, these data
164 demonstrate that Nb infection promotes substantial changes in lung monocyte and
165 macrophage subset dynamics. Further, these data suggest that the early influx of
166 monocytes observed in the lung may help to support the overall increases in lung
167 macrophage populations observed post-infection.

168 Our previous studies have shown that by day 7 after Nb inoculation sort-purified
169 lung macrophages can effectively kill infectious Nb larvae (L3) following in vitro culture
170 and can mediate accelerated resistance when transferred to otherwise naïve recipients[3].
171 Importantly, these bulk macrophage populations are comprised of both AMs and NAMs.
172 However, whether these two macrophage subsets equally or preferentially contribute to

173 parasite killing remains unknown. To test this, at day 7 after Nb inoculation, lung cell
174 suspensions were prepared as previously described[3], and AMs and NAMs were sort-
175 purified. Individual macrophage subsets ($1x10^6$/ml) were then cultured with exsheathed
176 L3 (100/well) in 24 well plates, for 5 days, as previously done with bulk macrophages[3].
177 As shown in **Fig. 2a**, AMs were approximately 5 times more effective at killing L3 than
178 NAMs. Assessment of parasite metabolic activity, by assaying their ATP amounts[3],
179 further showed significantly decreased activity in cultures seeded with AMs compared to
180 cultures seeded with NAMs (**Fig. 2b**). Previous studies have shown that Arg1 production
181 by macrophages is essential for the effective killing of parasitic larvae both in vitro and in
182 vivo[6,8]. Therefore, to investigate whether the macrophage killing observed correlated with
183 Arg1 production, AMs and NAMs were assessed for cytoplasmic Arg1 expression at 7
184 days after Nb infection. As shown in **Fig. 2c**, more than 10% of AMs expressed Arg1
185 after infection, while less than 3% of NAMs from treated mice expressed Arg1, consistent
186 with NAMs being less effective in killing L3. Furthermore, the total number of Arg1
187 expressing AMs was significantly greater post-infection while the numbers of Arg1-
188 expressing NAMs remained unchanged (**Fig. 2d**). Collectively, these studies indicate that
189 AMs mediate the majority of the parasite killing capacity within lung macrophage
190 compartments and that elevated cytoplasmic Arg1 protein expression is associated with
191 that enhanced capacity in a subset representing ~10% of the total AM compartment.
192 Our previous studies showed that the transfer of bulk lung macrophages from Nb
193 primed mice into otherwise naïve recipients was sufficient to mediate accelerated
194 resistance similar to the memory response observed after secondary challenge[3]. To
195 examine whether AMs also showed preferential resistance in vivo, AMs and NAMs were

196 sort-purified from the lungs of donor mice at day 7 after Nb inoculation and transferred to
197 naïve recipient mice, which were then inoculated with Nb. Unexpectedly, as shown in **Fig.**
198 **3a**, both AMs and NAMs were equally effective at mediating accelerated acquired
199 resistance in recipient mice at 5 days after Nb inoculation. Given that the NAMs expressed
200 low Arg1 relative to the AMs, this raised the possibility that the transferred NAMs were
201 differentiating into an AM-like subset that acquired the ability to preferentially upregulate
202 Arg1 and kill invading parasitic larvae. To test whether NAMs could develop an AM-like
203 phenotype in the lung, we isolated AMs and NAMs from CD45.1 donor mice at day 7 after
204 Nb inoculation and transferred these subsets intratracheally to naïve congenic CD45.2
205 recipients. Recipient mice were rested 2 days, inoculated with Nb and 5 days later lung
206 cell suspensions were collected and assessed for donor and recipient AM populations.
207 As shown in **Fig. 3b**, transferred CD45.1 donor NAMs gave rise to a substantial number
208 of macrophages with an AM-like phenotype (CD45.1$^{+}$, CD64$^{+}$,F4/80$^{+}$,SiglecF$^{+}$, CD11c$^{+}$)
209 that represented about 10% of the total AM population in the CD45.2 congenic recipients.
210 These data suggest that monocyte-derived macrophages contained within the NAM
211 compartment may possess the capacity to acquire an AM-like phenotype. To further
212 investigate the contribution of monocytes to the AM compartment post-Nb, we obtained
213 CCR2 GFP reporter and CCR2 Diphtheria toxin receptor (DTR) depleter mice. As early
214 as day 1 after Nb inoculation, CCR2$^{+}$ monocytes were increased several fold in the lung
215 and these high levels were sustained as late as day 7 after Nb inoculation (**Fig. 3c**).
216 These data further support our findings presented in **Fig. 1b** and highlight the significant
217 recruitment of monocytes into the lung shortly after Nb inoculation. To further examine
218 the extent to which monocytes contributed to the overall lung macrophage population

219 after infection, CCR2$^{DTR}$ mice were inoculated with Nb and administered DT at -1, 1, and
220 3 days post-infection to deplete monocytes and monocyte-derived macrophages. As
221 expected, NAMs were significantly reduced on day 7 post-infection after DT
222 administration (**Fig. 3d**), further corroborating a substantial contribution of monocytes to
223 the NAM compartment. However, intriguingly, AMs also showed a marked reduction in
224 their expansion typically observed after Nb inoculation (**Fig. 3e**). These data are
225 consistent with a role for monocyte-derived cells contributing to the population expansion
226 of AMs post-infection (**Fig. 3e**). To confirm the selective depletion of DT treatment on
227 CCR2$^{+}$ monocyte-derived macrophages post-DT treatment, a separate myeloid
228 population, eosinophils, which are CCR2$^{-}$, were also assessed. Eosinophils were also
229 increased in the lung at 5 days after inoculation but were not affected by DT administration
230 consistent with the specificity of the treatment (**Fig. 3f**). In aggregate, these data suggest
231 that lung infiltrating monocytes can acquire a tissue-resident AM phenotype and
232 contribute substantially to the increased AM population observed post-infection.
233 However, the contributions of these monocyte-derived AMs to host protection remained
234 unknown.
235 To further explore the characteristics and functional significance of monocyte-derived
236 alveolar macrophages (Mo-AMs), we employed established fate mapper mice that allow
237 monocyte-derived cells in adult mice to be identified by their history of *Cx3cr1*
238 expression[24]. With this mouse model, monocytes can be tracked in *Cx3cr1*$^{CreERT2\text{-}IRES\text{-}YFP}$
239 mice (abbreviated as *Cx3cr1*$^{Cre}$ mice), which express a tamoxifen (TAM)-inducible Cre
240 recombinase (CreERT2) under the control of the endogenous promoter, followed by an
241 IRES–EYFP element[24,25].

242 To track the fate of the CX3CR1$^{+}$ monocytes, *Cx3cr1*$^{Cre}$ mice were crossed with
243 *Rosa26*stop$^{-tdTomato}$ reporter mice (abbreviated as *R26*tdTomato mice), as previously
244 described[24]. The resultant *Cx3cr1*$^{CreERT2\text{-}IRES\text{-}YFP/+}$*Rosa26*$^{floxed\text{-}tdTomato/+}$ mice were
245 inoculated with Nb and administered TAM at day -1 and day +1 post-infection, which
246 irreversibly labels CX3CR1$^{+}$ cells and their progeny by inducing the expression of
247 tdTomato. As a control, naïve *Cx3cr1*$^{CreERT2\text{-}IRES\text{-}YFP/+}$*Rosa26*$^{floxed\text{-}tdTomato/+}$ mice were also
248 administered TAM (**Fig. 4a**). At day 7 after inoculation, lung cell suspensions were
249 collected and stained for markers associated with conventional AMs
250 (CD64$^{+}$,F4/80$^{+}$,SiglecF$^{+}$,CD11c$^{+}$) (**Fig. 4b - 4c**). The gated AM subset was then analyzed
251 for tdTomato expression. As shown in **Fig. 4d**, ~30% of AMs were tdTomato$^{+}$ post-Nb
252 infection, indicating that these cells are derived from CX3CR1$^{+}$ monocytes, while AMs
253 from naïve controls similarly treated with tamoxifen showed less than 1% tdTomato
254 expression (**Supplementary Fig. 1a,b**). Interestingly, tdTomato$^{+}$ positive cells persisted
255 for up to a month post-infection (**Fig. 4e**) and appeared phenotypically distinct from
256 tdTomato negative AMs by ultrastructural analysis (**Fig. 4 f**). Importantly, the use of these
257 fate mapping mice obviated the need for cell transfers and/or generation of chimeras for
258 tracing development of Mo-AMs, providing a useful more physiological method for
259 tracking and isolating Mo-AMs and tissue-derived (TD) AMs. Next, we sort-purified TD-
260 AMs (tdTomato$^{-}$) and Mo-AMs (tdTomato$^{+}$) at day 7 after Nb inoculation and cultured
261 them with Nb L3 to test whether they possessed common or unique anti-helminth effector
262 activity. Importantly**,** tdTomato$^{+}$ AMs derived from CX3CR1$^{+}$ monocytes were significantly
263 more effective at impairing L3 metabolic activity (quantified by decreased ATP) and killing
264 Nb larvae than their tissue-derived counterparts (**Fig. 4g,h**). These studies thus indicate

265 that after Nb inoculation, monocytes enter the lung and transition to an AM-like phenotype
266 by acquiring expression of Siglec-F and CD11c. However, these data also suggest that
267 monocyte-derived AM entering the lung post-infection are functionally distinct cells that
268 preferentially damage and kill invading helminth larvae.

269 To examine the localization of Mo-AMs in lung tissue during Nb infection,
270 *Cx3cr1*$^{\text{CreERT2-IRES-YFP/+}}$*Rosa26*$^{\text{floxed-tdTomato/+}}$mice were administered TAM as described
271 above and inoculated with Nb or left untreated. Bronchioalveolar lavage (BAL) was
272 collected at day 7 after Nb inoculation. As shown in **Supplementary Fig. 1c**, Mo-AMs
273 were not detected in BAL of uninfected mice, but were readily detectable in the BAL after
274 Nb inoculation. In contrast, TD-AMs were readily detectable in BAL in untreated and Nb
275 inoculated mice, with little change after infection (**Supplementary Fig. 1d**). Remaining
276 lung tissue after collection of BAL was also assessed and although Mo-AMs were not
277 observed in uninfected mice as expected, Mo-AMs and TD-AMs were readily detectable
278 after infection (**Supplementary Fig. 1c,d**). The presence of both AM subsets in
279 remaining lung tissue may be in part due to residual alveolar macrophages in alveoli and
280 airways after lavage as well as potential disruption of lung architecture resulting from
281 infection. The in situ distribution of Mo-AMs was also assessed after secondary
282 inoculation. As shown in **Supplementary Fig.1e**, marked increases in Mo-AMs in the
283 BAL were detected after secondary inoculation, compared to primary inoculation.
284 Collectively, these data suggest that Mo-AMs have populated the lung and are ideally
285 positioned to encounter invading parasitic larvae following a secondary challenge.

286 To visualize potential interactions between macrophages and larvae,
287 immunofluorescent staining of cryosections from Cx3cr1$^{\text{CreERT2-IRES-YFP/+}}$*Rosa26*$^{\text{floxed-}}$

288 $^{tdTomato/+}$mice was assessed after Nb secondary inoculation. In these experiments, the
289 second inoculation was administered 2 days after the first inoculation and mice were
290 sacrificed 6 days after primary inoculation. This approach optimized visualization of
291 trafficking parasites, as parasites are rapidly killed if the second inoculation is given at
292 later time points and are thus not readily visualized. As shown in **Fig. 4i**, using confocal
293 microscopy, Mo-AMs (tdTomato$^+$, CD11c$^+$; yellow-orange) are observed immediately
294 surrounding the parasite after a second infection, whereas TD-AMs (tdTomato$^-$
295 ,CD11c$^+$;green) are more restricted to the airways. tdTomato$^+$, CD11c$^+$ cells (Mo-AMs)
296 are also found in the airways consistent with our flow cytometric analysis of BAL fluid. It
297 should be noted that >98% of tdTomato$^+$, CD11c$^+$ cells exhibited an AM-like phenotype
298 (F480$^+$, CD64$^+$, CD11c$^+$, Siglec-F$^+$) as determined by flow cytometric analysis
299 (**Supplementary Fig. 1 f,g**).

300 Our findings that these Mo-AMs exhibit enhanced anti-helminth activity provokes
301 the hypothesis that they are phenotypically distinct from their tissue-derived counterparts.
302 To further test this, tdTomato$^+$ Mo-AMs and tdTomato$^-$ TD-AMs were administered TAM
303 (as in **Fig. 4a**), sort-purified on day 7 after Nb inoculation and subjected to global
304 transcriptome profiling. RNA-seq analysis showed that Mo-AMs had a gene expression
305 profile distinct from TD-AMs (**Fig. 5a**). Even by day 14 post-infection Mo-AMs maintained
306 distinct profiles relative to TDAMs and naïve AMs, as determined by pairwise Euclidean
307 distance calculation (**Fig. 5a**) and principal components analysis (**Fig. 5b**). Visualization
308 of overall expression patterns by volcano plots showed more transcriptionally regulated
309 genes in Mo-AMs compared to TD-AMs at day 7 and day 14 (**Fig. 5c**). Venn diagrams
310 of upregulated (**Supplementary Fig. 2a**) and downregulated (**Supplementary Fig. 2b**)

311 genes further illustrated the distinct differences in expressed genes between Mo-AMs and
312 TD-AMs after Nb inoculation. Ingenuity Pathway Analysis (IPA) further suggested that the
313 TD- and Mo-AMs were functionally distinct (**Supplementary Fig. 2c**). Importantly,
314 canonical type 2 pathways that are critical in mediating helminth resistance were more
315 pronounced in Mo-AMs relative to TD-AMs (**Fig. 5d**). Specifically, Arg 1, Retnla, Il-13,
316 and Mgl2 were all increased in Mo-AMs relative to TD-AMs on day 7 and to a lesser extent
317 on day 14 post-infection (**Fig. 5d**). While Mo-AMs remained heightened in these
318 responses on day 14 post-infection, TD-AMs had returned to baseline levels or in some
319 cases below baseline levels by this timepoint (**Fig 5d**). These data suggest that Mo-AMs
320 develop a potent M2-associated phenotype with anti-helminth functions. Additionally,
321 wound healing markers showed a similar pattern of increased expression in Mo-AMs
322 (**Supplementary Fig. 2d**). Notably, peroxisome proliferator-activated receptor gamma
323 (PPARγ) associated signaling pathways, important in lipid metabolism and surfactant
324 homeostasis[26], were instead significantly reduced in Mo-AMs relative to naïve TD-AMs at
325 day 7 ($\log_2$ fold change -1.72; FDR $p<0.001$) and day 14 ($\log_2$ fold change -1.95; FDR
326 $p<0.001$)) after Nb inoculation. This may reflect a more prominent role for TD-AMs in
327 homeostatic function associated with lipid metabolism.

328 In independent experiments, we also employed transposase-accessible chromatin
329 with sequencing (ATAC-seq) to examine changes in chromatin profiles by identifying
330 transposase-accessible regulatory gene elements in both TD- and Mo-AMs subsets on
331 day 7 post-infection. At a global level, the chromatin profiles of TD-AM from Nb inoculated
332 mice were more similar to naïve alveolar macrophages than Mo-AMs from Nb inoculated
333 mice as indicated by Euclidean distance calculation (**Supplementary Fig. 3a**) and

334 principal component analyses (**Supplementary Fig. 3b**). Differential volcano plot
335 analyses revealed greater accessibility of regulatory elements in the Mo-AMs from Nb
336 inoculated mice (**Supplementary Fig. 3c**), consistent with their increased overall
337 transcription levels as observed with RNAseq (**Fig. 5a-d**). Comparison of differentially
338 called peaks in the four replicates of Mo-AMs versus TD-AMs identified 33,229
339 differentially expressed peaks (**Supplementary Fig 3d**). No significant differences were
340 seen in chromatin accessibility between *Il33*. However, Mo-AMs had significant increases
341 ($p<0.001$) in chromatin accessibility at the *Arg1, Mgl2,* and *Retnla* promoter loci **(Fig 5e)**.
342 These findings suggest that the regulation of differential gene expression in TD-AMs is
343 mediated at the level of chromatin accessibility. These data correlate with the increased
344 *Arg1*, *Mgl2*, and *Retnla* transcripts also observed in the Mo-AMs (**Fig. 5d**).
345 Analyses of in vivo proliferation of macrophage subsets showed similar levels of
346 proliferation between TD-AMs and Mo-AMs at day 7 and day 14 after inoculation
347 (**Supplementary Fig. 4a,b**), consistent with both populations undergoing expansion in
348 part through cell cycling. However, Seahorse real-time cell metabolic analyses using the
349 mitochondria stress test revealed a higher oxygen consumption rate (OCR) and a higher
350 extracellular acidification rate (ECAR), in Mo-AMs compared to TD-AMs at day 7 after
351 inoculation (**Supplementary Fig. 4c**), indicating increased oxidative phosphorylation.
352 We also observed increased *Il13* mRNA in both alveolar macrophage subsets after Nb
353 inoculation. To corroborate these findings, we assessed IL-13 protein cytoplasmic
354 staining and observed significant increases in IL-13 in alveolar macrophages from Nb but
355 not *IL-4Ra*$^{-/-}$ mice at day 7 after inoculation (**Supplementary Fig. 4d**). These data are
356 consistent with previous reports of lung macrophages producing IL-13[27].

357 Collectively, our discovery-based studies revealed preferentially elevated levels of
358 *Arg1* gene expression in Mo-AMs, which were also most effective at killing L3 (**Fig 5d**).
359 To corroborate these findings, we performed qPCR on tdTomato$^{+}$ Mo-AMs and tdTomato$^{-}$
360 TD-AMs obtained from total lungs of *Cx3*cr1$^{\text{CreERT2-IRES-YFP/+}}$Rosa26$^{\text{floxed-tdTomato/+}}$ mice 8
361 days after L3 inoculation. As shown in **Fig. 6a**, Arg1 mRNA was markedly elevated in
362 tdTomato$^{+}$ Mo-AMs relative to controls. To assess whether Arg1 protein was similarly
363 increased in this subpopulation, Mo-AMs and TD-AMs were assayed for intracellular Arg1
364 protein expression by flow cytometric analysis. As shown in **Fig. 6b,c**, Arg1 protein was
365 expressed at considerably higher levels in FACS gated tdTomato$^{+}$ Mo-AMs relative to
366 tdTomato$^{-}$ TD-AMs We further corroborated these findings through cytology and
367 immunofluorescent staining of alveolar macrophage subsets that showed preferential
368 staining for Arg1 in Mo-AMs (**Supplementary Fig. 5**).
369 M2 macrophage activation is regulated by several factors including the production
370 of type 2 cytokines by specialized innate immune cells. More specifically, our work and
371 that of others have shown that neutrophils can contribute to M2 cell activation[3,7].
372 Therefore, we sought to assess whether the high Arg1 expression was also dependent
373 on Nb-activated neutrophils. A role for neutrophils in preferential activation of Mo-AMs
374 would be consistent with a role for extrinsic signals in addition to intrinsic cell lineage
375 differences contributing to differential macrophage subset activation in the lung. To test
376 this possibility, *Cx3cr1*$^{\text{CreERT2-IRES-YFP/+}}$*Rosa26*$^{\text{floxed-tdTomato/+}}$mice were administered TAM
377 as described above and anti-Ly6g neutrophil depleting Ab or isotype control was
378 administered at days -1, +1, and day 3 after Nb inoculation. At day 5 after inoculation total
379 lung cell suspensions were stained for AMs and analyzed by flow cytometry for tdTomato

380 expression. Elevations in intracellular Arg1 protein expression (**Fig. 6d-f**) and gene
381 expression (**Fig. 6g**), as measured by RT-PCR, were significantly reduced in tdTomato$^{+}$
382 Mo-AMs after neutrophil depletion.

383 Previous studies have shown that macrophage mediated helminth killing is
384 dependent on Arg enzymatic activity through use of specific inhibitors[3,8]. We next
385 examined macrophages from Arg1 conditional knockout mice, where macrophages were
386 isolated from Tie2-Cre Arg1$^{fl/fl}$ or control Tie2-Cre mice at day 7 after inoculation and
387 cultured with Nb L3. Use of Tie-2 to drive macrophage deletion of *Arg1* has significant
388 advantages over LysMCre, which is ineffective at deleting *Arg1* in macrophages[28]. As
389 shown in **Figure 7a,b**, macrophages from Nb primed Tie2-Cre *Arg1*$^{fl/fl}$ mice showed
390 markedly impaired L3 killing and corresponding increases in metabolic activity as
391 assessed by ATP worm levels. This is consistent with previous studies showing reduced
392 impairment of *Heligmosomoides polygyrus* larval mobility by macrophages from Tie2-
393 CreArg1$^{fl/fl}$ mice[11]. However, it remained unknown how Arg1 actually affects parasitic
394 nematode larval survival. Arg1 triggers a cascade of effects resulting in production of
395 potentially toxic urea and also polyamines, which can promote cellular activation and
396 proliferation[20]. Recent studies of the intestinal and hepatic type 2 responses in
397 Schistosome-infected mice have further shown an important role for Arg1 in depleting
398 local arginine concentrations, and thereby attenuating activation of nearby immune cells,
399 effectively resulting in immunosuppression[21]. Arginine depletion and not metabolite
400 generation mediated the downregulatory effect[29]. Based on these findings, we
401 hypothesized that one mechanism through which Arg1 may kill L3 would be through
402 localized depletion of arginine, an essential amino acid for nematodes, as they are

403 generally not thought to be capable of arginine biosynthesis[30,31]. To test whether L-
404 arginine was depleted in the macrophage/L3 cocultures L-arginine was directly measured
405 following culture of L3 alone, or coculture of exsheathed L3 with either naïve lung
406 macrophages or lung macrophages from mice inoculated with Nb for 7 days. Significant
407 decreases in L-arginine were detected only in L3 cocultures with lung macrophages from
408 Nb inoculated mice (**Fig. 7c**). We next performed L-arginine add back experiments to
409 examine whether macrophage killing could be blocked by supplementing the media with
410 highly purified L-arginine. As shown in **Fig. 7d, e**, larval killing was significantly decreased
411 with increased L-arginine supplementation and live parasite metabolic activity, as
412 measured by ATP values, was markedly increased. To assess whether L-arginine was
413 required for L3 survival under in vitro conditions, exsheathed larvae were cultured in
414 arginine-free media. As shown in **Fig 7f**, parasite mortality was high in arginine-free
415 media, while addition of arginine significantly reduced mortality. Furthermore,
416 supplementation of arginine free media with exogenous L-arginine enhanced parasite
417 ATP levels (**Fig. 7g**). To examine whether anti-helminth functions of lung macrophages
418 were specific to Nb, primed lung macrophages isolated at day 7 after Nb inoculation were
419 cocultured with a different nematode parasite, *H. polygyrus*. L3 mortality (**Fig. 7h**) was
420 markedly increased and was reduced by supplementation with L-arginine. Similarly
421 reduced L3 ATP levels were markedly enhanced by L-arginine administration (**Fig. 7i**).
422 These studies thus indicate that Nb-primed macrophages are capable of killing other
423 nematode parasite species and provide substantial insight into the protective
424 mechanisms of M2 macrophages.
425

426 **Discussion:**

427 Macrophages mediate resistance to helminths as well as microbial pathogens. Recent
428 studies suggest that the lung is an important target for therapeutic strategies and vaccine
429 development against helminths[2], and that lung macrophages with anti-helminth effector
430 functions develop shortly after Nb infection[3]. Tracking monocyte recruitment to the lungs
431 and their differentiation in this microenvironment, we showed that during infection they
432 can develop an alveolar macrophage-like phenotype that is distinct from TD-AMs and that
433 preferentially mediates helminth killing and includes expression of high levels of Arg1,
434 which is critical for helminth resistance. Development of this polarized Mo-AM phenotype
435 was dependent on neutrophil help and our studies further show that macrophage-derived
436 Arg1 mediates parasite killing through localized depletion of arginine, providing a
437 previously unappreciated nutrient deprivation mechanism for macrophage-mediated
438 helminth killing.

439 Emerging studies have now demonstrated that macrophages exhibit tissue-specific
440 phenotypes that are ideally suited for their specific microenvironments[18,24,32,33]. In the
441 lung, TD-AMs play a critical role in lung homeostasis including clearance of debris and
442 surfactant recycling[16,34]. After Nb infection, the lung NAMs are a heterogeneous
443 population, with macrophages derived and from monocytes and also tissue-derived
444 interstitial macrophage populations [17]. Our findings with the CCR2-DTR mice, and also
445 with the transfer experiments using CD45 congenic mice, now indicate that the rapid
446 increase in alveolar macrophages observed after Nb infection is supported by monocyte-
447 derived cells. Furthermore, these Mo-AMs are differentially activated with distinct effector
448 functions including enhanced parasite killing and Arg1 expression, thereby explaining why

449 NAMs were less effective at killing the helminths in vitro, but after transfer, in the context
450 of the lung microenvironment, could develop this anti-helminth effector function
451 associated with their expression of AM surface markers. Recent studies in a chimeric
452 model showed that recruited Mo-AMs during influenza infection preferentially conferred
453 protection against heterologous bacterial infections[18]. Interestingly, fibrosis was also
454 linked to a recruited Mo-AM population with increased Arg1 expression in an acute lung
455 injury model [19]. Our studies now show that tracking of monocytes, using fate mapping
456 mice under physiological conditions, reveals their differentiation into Mo-AMs that are
457 characterized by high Arg1 expression and enhanced anti-helminth effector function.
458 Parasites typically leave the lung and migrate to the small intestine by day 4 after
459 inoculation[35]. The magnitude of the type 2 inflammatory response decreases shortly
460 thereafter, but still remains potent, resulting in chronic inflammation and the associated
461 development of fibrosis and emphysematous pathology[36,37]. Mo-AMs expressed high
462 levels of CD11c and Siglec-F by day 7 but transcriptome analyses revealed that they were
463 distinct from TD-AMs as revealed by PCA and Euclidean distance analyses. The
464 observation that this population expressed considerably higher levels of Arg1 and other
465 type 2 markers compared to TD-AMs indicates a distinct activation state and effector
466 function. By day 14, upregulated gene expression of immune response genes was
467 decreased in the TD-AMs, while Mo-AMs retained relatively high expression of these
468 genes that including type 2-associated molecules. These findings are consistent with a
469 model where TD-AMs revert back to a housekeeping phenotype shortly after infection,
470 likely to assume their critical function of maintaining homeostasis and healthy lung
471 function[16]. In this context, as described in the Results, PPARγ expression remained

472 higher in TD-AMs at both day 7 and day 14 after Nb inoculation relative to Mo-AMs.
473 PPARγ mediates lipid metabolism, a critical homeostatic function of TD-AMs[16,26].
474 However, our findings may also be consistent with recent findings that TD-AMs may
475 undergo paralysis associated with poor phagocytic activity after bacterial infections[38].
476 Further studies of TD-AM function after helminth infection are needed to distinguish
477 between these possibilities. In contrast AMs derived from monocytes maintain a more
478 activated phenotype with high expression of M2 markers and associated remodeling of
479 the chromatin landscape. As such the Mo-AMs are likely primed to respond to
480 subsequent helminth infections. In future studies it will be interesting to examine the
481 duration of changes in the chromatin landscape relative to gene expression, as these
482 epigenetic modifications may potentially contribute to trained immunity, consistent with
483 previous studies showing persistence of trained macrophages as late as 45 days after Nb
484 inoculation[3]. These epigenetic changes in macrophages may also affect heterologous
485 infections, consistent with previous studies that Nb infection can enhance susceptibility
486 to infection with Mycobacterium tuberculosis in part through impaired macrophage
487 effector function[39]. Interestingly, we also observed increases in macrophage expression
488 of IL-13, which was confirmed by cytoplasmic IL-13 staining. Previous studies have also
489 shown increased lung macrophage IL-13 production during type 2 responses, in some
490 cases directly contributing to the polarization of the response[27,40]. It is increasingly
491 apparent that a number of different innate myeloid and lymphoid immune cells can
492 express type 2 cytokines during allergic and helminth responses, likely triggered by
493 activation of common pathways including IL-4R signaling[10], and potentially playing
494 essential roles at different stages of the response.

495 After primary infection, our findings show that several days elapse as the monocytes are
496 recruited to the lung and differentiate to the alveolar macrophage phenotype. The Mo-
497 AM population likely has little effect on parasite migration during a primary infection,
498 consistent with most parasites successfully reaching the small intestine by day 4 after
499 primary inoculation. However, after infection, the Mo-AMs persist in the lung for prolonged
500 periods: they are readily detected as late as 30 days after infection (data not shown). As
501 such, during a subsequent infection, parasites can encounter these macrophages in the
502 lung, slowing their migration and eventually culminating in their morbidity and death in the
503 lung over a period of several days, thereby blocking their migration to the intestine. Our
504 findings further suggest that the Mo-AMs play a critical role in contributing to this
505 accelerated resistance, likely through their heightened Arg1 activity, which depletes L-
506 arginine levels. We now show that these Mo-AMs are in close proximity to Nb larvae in
507 the lung after infection. Whether the macrophages simply adhere to the parasite as it
508 migrates through the lung, the larvae are trapped in aggregates of macrophages after
509 infection, or the macrophages potentially swarm the parasite is unknown. It should be
510 noted that increased Mo-AM activation including expression of additional genes
511 associated with type 2 immunity may also trigger other effector mechanisms contributing
512 to anti-helminth effects. The overall primed state of Mo-AMs may also play a significant
513 role in infections with heterologous pathogens, potentially providing protective immunity
514 or alternatively increased susceptibility as has been observed with *Mycobacterium*
515 *tuberculosis* infections[39]. As such, heterogeneity between individuals in innate responses
516 to specific pathogens may be potentially influenced by previous heterologous pathogen
517 exposure. The genetic background of the host may also be of importance and our studies

518 of Mo-AMs have necessarily focused on BL/6 mice as that is the genetic background of
519 the fate mapping mice used in these studies. Previous studies have shown potent type
520 2 responses to *N. brasiliensis* in both BL/6 and BALB/c mice[3,6,36]. In future studies, the
521 role of Mo-AMs in mediating helminth resistance in mice with varying genetic
522 backgrounds should be investigated.
523 Neutrophils are increasingly recognized as significant players in helminth infections and
524 in cross talk with macrophages. Recent studies indicate that neutrophils exhibit a distinct
525 alternatively activated (N2) phenotype during helminth infections[3] and that they can
526 contribute resistance mechanisms leading to reduced worm burden after primary
527 inoculation[4,5]. Interactions of macrophages with neutrophils can promote M2 activation,
528 likely through both production of type 2 cytokines and direct cell-cell interactions involving
529 efferocytosis[3,7]. Also, in the lung environment, surfactant protein A can also promote M2
530 macrophage activation[41]. Interestingly antibodies are not required for resistance to Nb[23],
531 although they do play an important role in resistance and macrophage Arg1 expression
532 during *H. polygyrus* infection[11,23]. The lung tissue microenvironment, including neutrophil
533 interactions, thus provides sufficient signals for M2 macrophage activation even in the
534 absence of Ab signaling. Effects of neutrophil-macrophage crosstalk in driving activation
535 and associated effector function of these myeloid cells can play a significant role in
536 immune responses against diverse pathogens[42]. Our findings indicate that neutrophils
537 are critical for the polarization of the Mo-AM subset towards elevated expression of type
538 2 markers, including Arg1. Our findings that neutrophils preferentially stimulate this
539 phenotype in recruited Mo-AMs indicates that both intrinsic lineage-specific activation

540 signatures and extrinsic signals provided in the inflamed lung tissue microenvironment
541 interact to drive their activation culminating in an anti-helminth effector phenotype.
542 Although previous studies have identified Arg1 as being essential in macrophage-
543 mediated helminth killing in the skin[8], lung[3], and small intestine[9,11], the mechanism
544 through which this enzyme mediates this effect has remained unknown. Our studies now
545 reveal a mechanism that is independent of the many molecules produced during the Arg1
546 cascade culminating in production of urea, ornithine and polyamines. Our findings do not
547 exclude other mechanisms involving the Arg1 pathways, or potentially other molecules
548 produced independently of Arg1. However, our studies do indicate that Arg1-mediated l-
549 arginine depletion is essential in macrophage-mediated killing of L3. The production of
550 high levels of Arg1 by macrophages as they surround the invading parasitic larvae
551 deprives the parasite of arginine. We now specifically show that Nb metabolism is slowed,
552 and mortality markedly increased in the absence of an external source of arginine in Nb
553 larval cultures with primed M2 macrophages. The developing L3 likely obtains this
554 essential amino acid from the vertebrate host as it traffics through various tissues in vivo.
555 The ability of the activated M2 macrophage to adhere to the invading L3 results in a
556 localized depletion of this critical nutrient, effectively providing a potent anti-helminth
557 effector mechanism. Our findings that arginine supplementation was sufficient to block
558 macrophage-mediated killing in both in vitro cultures and in vivo indicates the potent effect
559 of this anti-helminth macrophage effector mechanism. Given the intense selection
560 pressure of helminths on vertebrate evolution, one can postulate that the high level of
561 Arg1 produced by M2 macrophages, specifically helminth activated Mo-AMs, may in part
562 be an adaptation resulting in a potent resistance mechanism against these multicellular

563 pathogens. In contrast, Arg1 does not appear to significantly impact lung immune cell
564 activation and inflammation during type 2 responses, including schistosome egg-induced
565 granuloma formation[43]. It is intriguing that in microbial infections arginine also plays a
566 critical role in resistance, through generation of nitric oxide synthase 2 activity resulting in
567 the production of anti-microbial nitric oxide. As such, arginine metabolism thus plays an
568 important role in mediating resistance against eukaryotic as well as microbial pathogens
569 although the mechanisms contributing to the protective response are quite different. The
570 mechanism of Arg1-mediated resistance is indeed more similar to Arg1-mediated
571 suppression of Th2 cell activation, where nutrient depletion also plays a major role.
572
573
574
575
576
577
578
579
580
581
582
583
584
585

586 **Material and methods**

587 **Mice**
588 BALB/c ByJ (CD45.1), BALB/c (CD45.2), *Rosa26*$^{\text{floxed-tdTomato}}$
589 and *Cx3cr1*$^{\text{CreERT2-IRES-YFP}}$ BL/6 mice were purchased from The Jackson Laboratory (Bar
590 Harbor, ME) and CCR2-DTR, CCR2-GFP, Tie 2-Cre and Tie2-Cre Arg$^{\text{fl/fl}}$ mice were all
591 bred and maintained in a specific pathogen-free, virus Ab-free facility at Rutgers New
592 Jersey Medical School Comparative Medicine Resources. Healthy 8-12 week old mice
593 were selected for treatment groups from purchased or bred colonies, without using
594 specific randomization methods or specific blinding methods. The studies have been
595 reviewed and approved by the Institutional Animal Care and Use Committee at Rutgers-
596 the State University of New Jersey. The experiments herein were conducted according
597 to the principles set forth in the Guide for the Care and Use of Laboratory Animals,
598 Institute of Animal Resources, National Research Council, Department of Health,
599 Education and Welfare (US National Institutes of Health).
600
601 **Parasite culture and inoculation of mice**
602 *N. brasiliensis* (Nb) L3 were maintained in a petri dish culture containing charcoal and
603 sphagnum moss. The larvae were isolated from cultures using a modified Baermann
604 apparatus with 400U penicillin, 400 µg ml$^{-1}$ streptomycin, and 400 µg ml$^{-1}$ Neomycin
605 (GIBCO, Rockville, MD) in sterile PBS, and then washed with sterile PBS three times.
606 Mice were inoculated subcutaneously with a 40µl suspension of 650 Nb L3. For *H.*
607 *polygyrus*, after propagation, L3 larvae were maintained in PBS at 4°C.
608
609 **Flow cytometry and adoptive transfer**
610 Lung tissue was washed with stirring at room temperature for 10 min in Hank's balanced
611 salt solution (HBSS) with 1.3 mM EDTA (Invitrogen), then minced and treated at 37ºC for
612 30 min. with collagenase (1 mg / ml; Sigma) in RPMI1640 with 10% fetal calf serum (FCS)
613 and with 100 µg / ml of DNase for 10 min. Cells were lysed with ACK (Lonza, Walkersville,
614 MD) to remove erythrocytes. Cells were blocked with Fc Block (BD Biosciences, San
615 Jose, CA), directly stained with fluorochrome-conjugated antibodies against CD45,F4/80,
616 CD64, CD11c, Siglec-F,CD11b,Ly6C, and analyzed by flow cytometry. For adoptive
617 transfer, macrophages (F4/80$^{+}$CD64$^{+}$SiglecF $^{\text{vari}}$CD11c $^{\text{vari}}$), alveolar macrophages (AMs)
618 (F4/80$^{+}$CD64$^{+}$SiglecF$^{+}$CD11c$^{\text{hi}}$), or nonalveolar macrophages (NAMs)
619 (F4/80$^{+}$CD64$^{+}$SiglecF$^{-}$CD11c $^{\text{vari}}$), were electronically sort purified (>98%), 5 million cells
620 were transferred i.t. into recipient mice. Two days after cell transfer, the recipients were
621 inoculated with Nb L3. For *Cx3cr1*$^{\text{CreERT2-IRES-YFP}}$ x *Rosa26*$^{\text{floxed-tdTomato}}$ reporter mice,
622 tamoxifen (75 mg/kg body weight, Sigma, cat#T5648) were delivered to mice at days -1,
623 and +1 after Nb inoculation. At different timepoints after inoculation, single cells were
624 isolated from whole lung and directly stained with fluorochrome-conjugated antibodies
625 against CD45, F4/80, CD64, CD11c, Siglec-F and analyzed by flow cytometry. Cells
626 were gated on CD45$^{+}$,F4/80$^{+}$,CD64$^{+}$ cells, then further gated on Siglec-F$^{+}$, CD11c$^{\text{hi}}$ AMs.
627 AMs were separated into tdTomato$^{+}$ monocyte-derived alveolar macrophages (Mo-AMs)
628 and tdTomato$^{-}$ alveolar macrophages (TD-AMs). For intracellular staining of Arg1, cells
629 were first surface stained and then fixed and permeabilized using a kit from BD
630 BioSciences (cat# 554714). For cytospin analyses, sorted cells (2 x10$^{5}$) from lung tissue

631 were suspended in 200 µl of 1X PBS with 2.5% FCS. The sorted cell suspensions were
632 loaded into a Shandon Cytospin 4 (Thermo Electron Corporation, Waltham, MA), spun at
633 800-1000 rpm for 5 min and stored at -80°C. Frozen cytospin slides were thawed at room
634 temperature for 30 min, fixed in 4% PFA for 15 min, and stained with an APC-conjugated
635 antibody specific to Arginase 1 or corresponding isotype control (Bioss Inc., Woburn, MA).
636 Coverslips were applied to the slides using Vectashield mounting medium (Vector
637 Laboratories, Burlingame, CA) with DAPI. Images were taken using a Leica DM6000B
638 fluorescent microscope, Orca Flash 4.0 mounted digital camera (Hamamatsu Photonics
639 K.K., Japan) and LAS Advanced Fluorescence software (Leica Microsystems, Buffalo
640 Grove, IL). Fluorescent channels were photographed separately and then merged.
641 Exposure times and fluorescence intensities were normalized to appropriate control
642 images.
643
644 **Confocal microscopy**
645 Cx3cr1$^{CreERT2\text{-}IRES\text{-}YFP/+}$Rosa26$^{floxed\text{-}tdTomato/+}$ received tamoxifen at day -1 and +1 after
646 primary Nb inoculation of 500 L3. At day 2 after primary inoculation, mice were given a
647 second inoculation of 250. Lung tissues were then collected at day 6 after primary
648 inoculation. This regimen was found to optimize visualization of migrating parasites
649 interacting with primed macrophages. Lung tissues were fixed in 1% paraformaldehyde
650 overnight at 4°C. Tissues were washed with 5mM $NH_4Cl$ and incubated in 30% (w/v)
651 sucrose overnight at 4°C. Lung tissue was embedded in Optimal Cutting Temperature
652 Compound (Tissue-Tek) and 5 µm sections were cut on CM1950 Cyrostat (Leica,
653 Weltzlar, Germany). Sections were blocked with 1% Rat serum and 1% FcBlock in PBS
654 for 1 hr, followed by 5ug/ml of anti-CD11c-APC overnight and sealed with ProLong Gold
655 Antifade (Invitrogen, Waltham, MA). Confocal Images were captured using a Nikon A1R
656 SI confocal microscope with the DUG GaAsP detector. 10x Plan Apo Lambda N.A. 0.45,
657 20x Plan Apo VC N.A. 0.75 and 60x Plan Apo VC N.A. 1.4 objectives were used along
658 with DIC optics for the transmitted light images.
659
660 **Electron microscopy**
661 Samples were fixed in 2.5% glutaraldehyde / 4% paraformaldehyde in 0.1M cacodylate
662 buffer and then post-fixed in buffered 1% osmium tetroxide. Samples were subsequently
663 dehydrated in a graded series of acetone and embedded in Embed812 resin. 90nm thin
664 sections were cut on a Leica UC6 ultramicrotome and stained with saturated solution of
665 uranyl acetate and lead citrate. Images were captured with an AMT (Advanced
666 Microscopy Techniques) XR111 digital camera at 80Kv on a Philips CM12 transmission
667 electron microscope.
668
669 **Macrophage co-cultures with parasitic L3**
670 Macrophages, alveolar macrophages, or nonalveolar macrophages, were electronically
671 sorted from mice inoculated with Nb for 7 days, and placed on 12-well plates (1 x $10^6$) in
672 2 ml of RPMI1640 medium with 10% of FBS, 400U penicillin, 400 µg/ml streptomycin,
673 and 100 µg/ ml gentamycin. 100 µl of serum from the donor mice was also added to
674 medium. One hundred ex-sheathed L3 larvae were added to each well. Cells and worms
675 were co-cultured for 5 days at 37°C. The procedure to ex-sheath larvae included
676 incubation of L3 with 6.7 mM sodium hypochlorite in PBS for 15 min. at room temperature,

677 washing the L3 six times with sterile PBS containing 400U penicillin and 400 µg
678 ml−1 streptomycin. To ex-sheath Hp L3, the larvae were maintained in phenol
679 RPMI1640 with 10% FBS at $37^0$C, and $CO_2$ was added to the medium until yellow color
680 obtained, and then incubated for 25hrs in $CO_2$ incubator. The ex-sheathed larvae were
681 isolated using a modified Baermann apparatus with 400U penicillin, 400 µg
682 $ml^{-1}$ streptomycin, and 400 µg $ml^{-1}$ Neomycin (GIBCO, Rockville, MD) in sterile PBS, and
683 then washed with sterile PBS three times. In some experiments, the L3 were cultured in
684 L-arginine free RPMI1640 (Thermofisher) without cells and in some groups commercial
685 L-arginine was added to the medium. The ATP levels for the L3 were performed according
686 to the manufacturer's instructions. Briefly, 20 Nb L3 were collected with 100 µl of PBS
687 and 100µl of the Celltiter-Glo Luminescent reagent (Promega, Madison, WI) was then
688 added. The larvae were homogenized and incubated for five minutes at room temperature
689 to stabilize the luminescence signal. After the homogenate was centrifuged at 1000g for
690 2 minutes, 100 µl of supernatant was applied to the luminometer to measure
691 luminescence. As a negative control, larvae in RPMI1640 medium were treated in boiling
692 water for five minutes and after cooling, the worms were homogenized with reagent. Dead
693 larvae after incubation with macrophages were defined as non-motile, outstretched
694 bodies, with non-refractive internal structures. L- arginine was measured using an L-
695 arginine assay kit (Abcam, cat#ab252892),
696
697 **Cytokine gene expression by RT-PCR**
698 For qPCR, RNA was extracted from lung tissue or sorted macrophages and reverse
699 transcribed to cDNA. qPCR was done with Taqman (Life Technologies Corporation,
700 Carlsbad, CA) kits and the Applied Biosystems QuantStudio 6 Flex Real-Time PCR
701 System. All data were normalized to 18S ribosomal RNA, and the quantification of
702 differences between treatment groups was calculated according to the manufacturer's
703 instructions. Gene expression is presented as the fold increase over naïve WT controls.
704
705 **RNA sequencing**
706 Alveolar macrophages from *Cx3*cr1$^{CreERT2\text{-}IRES\text{-}YFP/+}$Rosa26$^{floxed\text{-}tdTomato/+}$ Nb- inoculated
707 mice were sort-purified by gating on $CD45^+$,$CD64^+$,F4/80+,$CD11c^+$,Siglec-$F^+$ AMs then
708 sorted based on tdTomato expression, with TD-AMs being $tdT^-$ and Mo-AMs $tdT^+$. Cells
709 from a minimum of three biological replicates were sorted and pooled. The purity of all
710 cell populations was 98% or greater. RNA was extracted using the RNeasy Plus Micro
711 Kit (catalog no. 74034; QIAGEN). Illumina-compatible libraries were generated using the
712 NEBNext Ultra II DNA Library Prep Kit for Illumina (catalog no. E7645S; New England
713 BioLabs) and sequenced using an Illumina NovaSeq 6000 system in a paired-end 2x50-
714 base pair (bp) reads configuration. Bulk RNA-seq analysis was performed in accordance
715 with the nf-core RNA-seq guidelines v.1.4.2[44]. Briefly, the output reads were aligned to
716 the GRCm38 (mm10) genome using STAR, followed by gene count generation using
717 feature Counts and StringTie[45-47]. Read counts were normalized and compared between
718 groups for differential gene expression using DESeq2 with significance cutoff at false
719 discovery rate-adjusted $p<0.05$[48]. Determination of functional pathways was performed
720 using Ingenuity Pathway Analysis (IPA) on differentially expressed genes.
721
722

723 **Assay for transposase-accessible chromatin with sequencing (ATAC-seq)**
724 Sorted cells were lysed in buffer (10 mM Tris-HCl, 10 mM NaCl, 3 mM $MgCl_2$,
725 0.1% octylphenoxypolyethoxyethanol, 0.1% digitonin and 0.1%IPGAL) for 3 min at 4°C
726 and then washed with lysis buffer without digitonin or IPGAL and centrifuged and
727 resuspended with transposase reaction mix (Ilumina Nextera), and incubated for 30 min
728 at 37°C. Cells were then PCR amplified in KAPA HiFi 2× mix (Kapa Biosystems) with
729 barcoding primers. Amplification was conducted for 45 s at 98°C, followed by five cycles
730 of denaturing at 98°C for 15 s, annealing at 63°C for 30 s, extension at 72°C for 30 s, and
731 a final extension of 72°C for 1 min in a thermal cycler (MX4005P). Quantitative PCR library
732 amplification test and PCR library amplification were performed as previously described[49].
733 Sequencing reads were trimmed (TrimGalore v0.6.4) and aligned to the reference
734 genome (GRCm38) using BWA (v0.7.17). Subsequent QC and filtering was performed
735 using picard (v2.23.1), SAMtools (v1.10), BEDtools (v2.29.2), and BAMtools (v2.5.1),
736 followed by peak calling using MACS2 (v2.2.7.1) and annotation via HOMER (v4.11).
737 Statistically significant differential peaks were identified between groups using DESeq2
738 (v1.26) and visualized using R.
739
740 **Seahorse Assay for metabolic activity**
741 *Cx3*cr1$^{CreERT2\text{-}IRES\text{-}YFP/+}$Rosa26$^{floxed\text{-}tdTomato/+}$ and CX3CR1-cre mice (control group)
742 received tamoxifen at one day before and one day after Nb inoculation (-1, +1 day) and
743 were sacrificed at day 7. Lung single cells were isolated and td tomato+ and td tomato-
744 alveolar macrophages from reporters or alveolar macrophages from control group mice
745 were sorted via flow cytometry. Alveolar macrophages (~75,000 cells/well) from each
746 group were seeded into CellTak (Corning, # 354240) coated XFp plates in XF RPMI
747 complete assay media, and incubated at 37°C without $CO_2$ for 45 minutes. The assay
748 was run on a Seahorse XFp Extracellular Flux Analyzer with each group of AMs run in
749 duplicate. After 20 cycles of basal measurement, Rotenone and Antimycin A (Seahorse
750 XF Cell Mito Stress Kit), inhibitors of mitochondrial complex I and III, respectively, were
751 injected into each well for a final concentration of 0.5 uM/well. Oxidative phosphorylation
752 was measured by the oxygen consumption rate (OCAR; pmol/min) while glycolysis was
753 measured by the extracellular acidification rate (ECAR; mpH/min) due to the
754 accumulation of lactate or other metabolic acids and release of protons into the
755 extracellular medium.
756
757 **5-Ethynyl-2´-deoxyuridine (EdU) incorporation assay**
758 *Cx3*cr1$^{CreERT2\text{-}IRES\text{-}YFP/+}$Rosa26$^{floxed\text{-}tdTomato/+}$ mice received tamoxifen at one day before
759 and one day after Nb inoculation (-1, +1 day), and received Edu (5mg/ml, 100 ul, i.p.)
760 every other day starting from one day before Nb inoculation ((-1, +1, +3, +5 day) and
761 sacrificed at day 7. Control groups received tamoxifen and Edu but were not inoculated
762 with Nb. Lung macrophages were stained with fluorochrome-conjugated antibodies
763 against CD45, F4/80, CD64, CD11c, Siglec-F, then Edu incorporation was assessed
764 using Click-iT Edu flow cytometry cell proliferation assay kit (ThermoFisher Scientific,
765 cat#C10424).
766
767
768

769 **Statistical analysis**
770 Data were analyzed using the statistical software program Prism 8 (GraphPad Software,
771 Inc., La Jolla, CA) and are reported as means (± SEM). Differences between two groups
772 were assessed by student's T-test, differences among multiple groups were assessed by
773 one way ANOVA and individual comparisons were analyzed using Holm-Sidak test.
774 Differences of $p < 0.05$ were considered statistically significant.
775
776
777
778
779 **Legends:**
780
781 Fig. 1 Substantial changes in lung macrophage subsets occurs after *N. brasiliensis*
782 inoculation.
783 Flow cytometric analysis of macrophage subsets obtained from single cell suspensions
784 of whole lungs from BALB/c mice at days 1, 7, and 14 after *N. brasiliensis* inoculation. (a)
785 Total numbers of lung macrophages ($CD64^+$, $F4/80^+$, $CD11c^{var}$); (b) monocytes
786 ($CD11b^+$,$Ly6C^+$); (c) alveolar macrophages (AMs), (CD64+,F4/80+,SiglecF+,CD11c+);
787 (d) non-alveolar macrophages (NAMs) ($CD64^+$,$F4/80^+$,Siglec-$F^-$,$CD11c^{var}$); (e)
788 eosinophils ($F4/80^+$,Siglec-$F^+$, $CD11c^-$). Each symbol represents an individual mouse and
789 horizontal lines indicate the mean. All results are representative of two independent
790 experiments. *p<0.05, **p<0.01.
791
792 Fig. 2 Alveolar macrophages preferentially contribute to parasite killing and express
793 high arginase.
794 (a, b) Lung alveolar macrophages (AMs) and nonalveolar macrophages (NAMs) were
795 stained as in Fig. 1 and sort purified from whole lung cell suspensions at day 7 after *N.*
796 *brasiliensis* inoculation of BALB/c mice. AMs and NAMs were seeded to 24-well plates
797 (1x $10^6$ cell/well) and co-cultured with 100 exsheathed third stage larvae (L3). At day 5
798 after culture, the percent mortality (a) and worm ATP concentration (b) were determined.
799 This experiment was repeated three times with similar results. (c, d) Representative flow
800 cytometry plots (c) and lung macrophage numbers (d) for cytoplasmic arginase protein
801 expression in AMs and NAMs at day 7 after *N. brasiliensis* inoculation. Each symbol
802 represents triplicates of pooled samples (a, b), or individual mice (d). All results are
803 representative of two independent experiments. **p<0.01
804
805 Fig. 3 Lung infiltrating monocytes acquire a tissue-resident phenotype and contribute to
806 the increased alveolar macrophage population after *N. brasiliensis* inoculation.
807 (a) At day 7 after *N. brasiliensis* (Nb) inoculation, donor macrophages including total
808 macrophages, alveolar macrophages (AMs), and non-alveolar macrophages (NAMs)
809 were electronically sorted and transferred to recipient mice, which were inoculated with
810 Nb two days later. Recipient mice were assayed for intestinal worm number at day 5 after
811 inoculation; a control group did not receive macrophages. (b) donor CD45.1 mice were
812 inoculated with Nb and 7 days later, lung NAMs and AMs (as described in Fig. 1) were
813 sort-purified and transferred i.t. into naive recipients (CD45.2), which were inoculated with
814 Nb 2 days later. Donor and recipient lung AM populations were assessed at day 5 after

Nb inoculation. Flow cytometry plots were representative of 3 mice per group and 2 independent experiments. (c) CCR2-GFP reporter mice were assessed by flow cytometric analysis for monocyte recruitment to total lungs at days 1 and 7 after Nb inoculation. (d-f) Monocytes were depleted by administration of DT at -1, +1, and +3 after Nb inoculation of CCR2-DTR mice. At day 5 after Nb inoculation, numbers of lung NAM (d), AM (e), and eosinophils (f) were determined by flow cytometric analysis. Each symbol represents an individual mouse and horizontal lines indicate the mean. All results are representative of two independent experiments. **$p<0.01$

Fig. 4. Monocyte-derived alveolar macrophages preferentially damage and kill *N. brasiliensis* L3.

(a-d) Fate-mapping of monocyte-derived macrophages recruited to the lung after *N. brasiliensis* (Nb) infection. *Five* mice were pulse administered tamoxifen at days -1 and +1 after Nb inoculation (Fig 1a). Whole lung was collected at day 7 after inoculation and single cell suspensions stained for alveolar macrophages (AMs) as described in Fig. 1. $F480^+$,$CD64^+$ lung macrophages were gated for expression of CD11c and Siglec-F (b,c) and double positive cells were in turn gated for tdTomato expression (d). (e) Whole lung cell suspensions from *Cx3*cr1$^{CreERT2\text{-}EYFP\text{-}IRES\text{-}YFP/+}$Rosa26$^{floxed\text{-}tdTomato/+}$ reporter mice were assessed for tdTomato $(tdT)^+$ monocyte-derived alveolar macrophages (Mo-AMs) at different timepoints after Nb inoculation. (f) $tdTomato^-$ and $tdTomato^+$ cells were sort-purified on day 30 post-infection and prepared for ultrastructural analysis via TEM (magnification 3800x) (g, h) Lung tdTomato $^+$ ($tdT^+$ AM) monocyte- derived AMs and $tdTomato^-$ (tdT-AM) tissue-derived AMs were sort purified from Nb-primed *Cx3*cr1$^{CreERT2\text{-}EYFP\text{-}IRES\text{-}YFP/+}$Rosa26$^{floxed\text{-}tdTomato/+}$ reporter mice at day 7 post-infection. Macrophage subsets were seeded to 24-well plates (1 x $10^6$ cell/well) and co-cultured with 100 exsheathed L3. At day 5 after culture, worm ATP concentration (g) and percent mortality (h) were determined. Triplicate samples were assayed from pools of 20 larva from each well for determination of ATP concentration. Each symbol represents mean of triplicate samples and this experiment was repeated three times with similar results. (i) Lungs from *Cx3*cr1$^{CreERT2\text{-}EYFP\text{-}IRES\text{-}YFP/+}$Rosa26$^{floxed\text{-}tdTomato/+}$ reporter mice were collected after a second inoculation with Nb., sectioned, and stained with APC-CD11c antibody for confocal Immunofluorescence imaging analysis of CD11c and CX3CR1 ($tdTomato^+$) expression. Image is representative of total 8 individual mice. White marker, Nb larvae; blue marker, $CD11c^+$, $CX3CR1^-$ TD-AMs, and red marker, $CD11c^+$, $CX3CR1^+$ Mo-AMs.

Fig. 5. Monocyte-derived alveolar macrophages have distinct phenotype characterized by upregulation of type 2 markers.

*Cx3*cr1$^{CreERT2\text{-}EYFP\text{-}IRES\text{-}YFP/+}$Rosa26$^{floxed\text{-}tdTomato/+}$ reporter mice received tamoxifen at days -1, and +1 after *N. brasiliensis* (Nb) infection. At day 7 and day 14, $tdTomato^+$ monocyte-derived alveolar macrophages (Mo-AMs) and $tdTomato^-$ tissue-derived AMs (TD-AMs) were sorted-purified for RNA-seq transcriptional analysis and compared to naïve AMs, with 3 mice/treatment group. (a) pairwise Euclidean distance relative to the transcriptional profiles, demonstrating sample relatedness between AMs from untreated mice, and Mo-AMs and TD-AMs at day 7 and 14 after Nb inoculation (b) Principal Component Analysis of transcriptional profiles of treatment groups; (c) volcano plots of TD-AMs and Mo-AMs individual gene expression profiles at day 7 and day 14 expressed as compared to AMs

861 from naïve mice; (d) Expression of selected characteristic type 2 response markers in TD-
862 AMs and Mo-AMs at day 7 and day 14 after Nb inoculation as expressed relative to AMs
863 from naïve mice($Log_2$ fold change); (e) Genome browser views of the *Arg1*, *Il33*, *Mgl2*
864 and *Retnla* in naïve, TD-AMs, and Mo-AMs. Each track represents the normalized read
865 counts of accessible chromatin regions.
866
867 Fig. 6 After *N. brasiliensis* infection, monocyte-derived alveolar macrophages
868 preferentially express arginase 1 which is dependent on extrinsic neutrophil signaling.
869 (a-c) *Cx3*cr1$^{CreERT2\text{-}EYFP\text{-}IRES\text{-}YFP/+}$Rosa26$^{floxed\text{-}tdTomato/+}$ reporter mice were administered
870 tamoxifen and inoculated with *N. brasiliensis* (Nb) as described in Fig. 5. (a) Arginase 1
871 (Arg1) mRNA levels by qPCR in subpopulations of lung alveolar macrophage (AM)
872 subsets at day 8 after Nb inoculation expressed relative to naïve AMs; (b) Representative
873 flow cytometric analysis of Arg1 intracellular protein expression in AM subsets at day 7
874 after Nb inoculation and (c) Arg 1 mean fluorescence intensity (MFI) in individual samples
875 from different treatment groups; (d-g) *Cx3*cr1$^{CreERT2\text{-}EYFP\text{-}IRES\text{-}YFP/+}$Rosa26$^{floxed\text{-}tdTomato/+}$
876 reporter mice were administered anti-Ly6G Ab or isotype control at days -1,1,and 3 and
877 given tamoxifen at days -1 and 1 after Nb inoculation. (d-f) representative flow cytometric
878 analyses of Arg1 intracellular protein expression after neutrophil depletion (f) Arg1 MFI in
879 individual samples from each treatment group. (g) Arg1 mRNA levels by qPCR in
880 macrophage subsets, presented as the fold increase over naïve AMs. Data shown are
881 the mean and SEM of triplicate samples (a) or of duplicated samples (g) from a pool of
882 four to eight mice per group and are representative of two independent experiments.
883 Each symbol represents an individual mouse and horizontal lines indicate the mean. All
884 results are representative of two independent experiments. *$p<0.05$, **$p<0.01$
885
886 Fig. 7 L-arginine depletion by Nb activated lung macrophages kills parasitic larvae
887 (a,b) Tie2-Cre (CRE) and Tie2-Cre Arg1$^{fl/fl}$ (Cre Arg1$^{fl/fl}$) mice were inoculated with Nb L3
888 and 5 days later total lung macrophages were sort purified and cultured ($1X10^6$ cells/well)
889 with 100 Nb exsheathed L3 and assayed for worm ATP (a) and percent mortality (b). (c)
890 Arginine levels in supernatant were measured in cultures with L3, or cocultures with sort-
891 purified naïve lung macrophages or lung macrophages isolated from Nb, at day 5 after
892 culture. (d,e) Sort purified total lung macrophages from Nb inoculated mice were
893 cocultured with Nb exsheathed L3 naïve macrophages and supplemented with L-arginine.
894 At day 5 after culture, the percent mortality (**d**) and larval ATP concentration (e) were
895 determined, as described in Fig. 4. (f, g) ex-sheathed Nb larva (100 L3) were seeded to
896 12 well plates and cultured with L-arginine free RPMI1640 media, with one group
897 supplemented with L-arginine. At day 3, 8, and 15 after culture, the percent mortality was
898 assessed (**f**), and remaining worm ATP concentration assessed at day 15 (**g**). Data are
899 presented as the mean and SEM of triplicate samples (f) or presented as individual
900 samples obtained from 20 larva from each well for determination of ATP concentration
901 and horizontal lines indicate the mean(g). (h,i) Total lung macrophages were sort-purified
902 from Nb inoculated mice as described above and co-cultured with L3. Percent mortality
903 (h) and worm ATP concentration (i) were assessed. In all experiments, each symbol
904 represents an individual mouse and horizontal lines indicate the mean. All results are
905 representative of ate least two independent experiments. *$p<0.05$, **$p<0.01$
906

## References


1. Gause, W.C., Wynn, T.A. & Allen, J.E. Type 2 immunity and wound healing: evolutionary refinement of adaptive immunity by helminths. *Nat Rev Immunol* **13**, 607-614 (2013).
2. Harvie, M.*, et al.* The lung is an important site for priming CD4 T-cell-mediated protective immunity against gastrointestinal helminth parasites. *Infect Immun* **78**, 3753-3762 (2010).
3. Chen, F.*, et al.* Neutrophils prime a long-lived effector macrophage phenotype that mediates accelerated helminth expulsion. *Nat Immunol* **15**, 938-946 (2014).
4. Bouchery, T.*, et al.* Hookworms Evade Host Immunity by Secreting a Deoxyribonuclease to Degrade Neutrophil Extracellular Traps. *Cell host & microbe* **27**, 277-289 e276 (2020).
5. Sutherland, T.E.*, et al.* Chitinase-like proteins promote IL-17-mediated neutrophilia in a tradeoff between nematode killing and host damage. *Nat Immunol* **15**, 1116-1125 (2014).
6. Chen, F.*, et al.* An essential role for TH2-type responses in limiting acute tissue damage during experimental helminth infection. *Nat Med* **18**, 260-266 (2012).
7. Bosurgi, L.*, et al.* Macrophage function in tissue repair and remodeling requires IL-4 or IL-13 with apoptotic cells. *Science* **356**, 1072-1076 (2017).
8. Obata-Ninomiya, K.*, et al.* The skin is an important bulwark of acquired immunity against intestinal helminths. *J Exp Med* (2013).
9. Anthony, R.M.*, et al.* Memory T(H)2 cells induce alternatively activated macrophages to mediate protection against nematode parasites. *Nat Med* **12**, 955-960 (2006).
10. Gause, W.C., Rothlin, C. & Loke, P. Heterogeneity in the initiation, development and function of type 2 immunity. *Nat Rev Immunol* (2020).
11. Esser-von Bieren, J.*, et al.* Antibodies trap tissue migrating helminth larvae and prevent tissue damage by driving IL-4Ralpha-independent alternative differentiation of macrophages. *PLoS Pathog* **9**, e1003771 (2013).
12. Scott, C.L., Henri, S. & Guilliams, M. Mononuclear phagocytes of the intestine, the skin, and the lung. *Immunol Rev* **262**, 9-24 (2014).
13. Gundra, U.M.*, et al.* Alternatively activated macrophages derived from monocytes and tissue macrophages are phenotypically and functionally distinct. *Blood* **123**, e110-122 (2014).
14. Jenkins, S.J.*, et al.* Local macrophage proliferation, rather than recruitment from the blood, is a signature of TH2 inflammation. *Science* **332**, 1284-1288 (2011).
15. Bleriot, C., Chakarov, S. & Ginhoux, F. Determinants of Resident Tissue Macrophage Identity and Function. *Immunity* **52**, 957-970 (2020).
16. Hussell, T. & Bell, T.J. Alveolar macrophages: plasticity in a tissue-specific context. *Nature reviews. Immunology* **14**, 81-93 (2014).
17. Ural, B.B.*, et al.* Identification of a nerve-associated, lung-resident interstitial macrophage subset with distinct localization and immunoregulatory properties. *Sci Immunol* **5**(2020).
18. Aegerter, H.*, et al.* Influenza-induced monocyte-derived alveolar macrophages confer prolonged antibacterial protection. *Nat Immunol* **21**, 145-157 (2020).

951 19. Misharin, A.V., *et al.* Monocyte-derived alveolar macrophages drive lung fibrosis and
952 persist in the lung over the life span. *J Exp Med* **214**, 2387-2404 (2017).
953 20. Kreider, T., Anthony, R.M., Urban, J.F., Jr. & Gause, W.C. Alternatively activated
954 macrophages in helminth infections. *Curr Opin Immunol* **19**, 448-453 (2007).
955 21. Pesce, J.T., *et al.* Arginase-1-expressing macrophages suppress Th2 cytokine-driven
956 inflammation and fibrosis. *PLoS Pathog* **5**, e1000371 (2009).
957 22. Katona, I.M., Urban, J.F., Jr. & Finkelman, F.D. The role of L3T4+ and Lyt-2+ T cells in the
958 IgE response and immunity to Nippostrongylus brasiliensis. *J Immunol* **140**, 3206-3211
959 (1988).
960 23. Liu, Q., *et al.* B cells have distinct roles in host protection against different nematode
961 parasites. *J Immunol* **184**, 5213-5223 (2010).
962 24. Gundra, U.M., *et al.* Vitamin A mediates conversion of monocyte-derived macrophages
963 into tissue-resident macrophages during alternative activation. *Nat Immunol* **18**, 642-
964 653 (2017).
965 25. Parkhurst, C.N., *et al.* Microglia promote learning-dependent synapse formation through
966 brain-derived neurotrophic factor. *Cell* **155**, 1596-1609 (2013).
967 26. Caputa, G., Castoldi, A. & Pearce, E.J. Metabolic adaptations of tissue-resident immune
968 cells. *Nat Immunol* **20**, 793-801 (2019).
969 27. Wu, K., *et al.* TREM-2 promotes macrophage survival and lung disease after respiratory
970 viral infection. *J Exp Med* **212**, 681-697 (2015).
971 28. Murray, P.J. Macrophage Polarization. *Annual review of physiology* **79**, 541-566 (2017).
972 29. Van de Velde, L.A., *et al.* T Cells Encountering Myeloid Cells Programmed for Amino
973 Acid-dependent Immunosuppression Use Rictor/mTORC2 Protein for Proliferative
974 Checkpoint Decisions. *J Biol Chem* **292**, 15-30 (2017).
975 30. Tyagi, R., Rosa, B.A., Lewis, W.G. & Mitreva, M. Pan-phylum Comparison of Nematode
976 Metabolic Potential. *PLoS Negl Trop Dis* **9**, e0003788 (2015).
977 31. Zecic, A., Dhondt, I. & Braeckman, B.P. The nutritional requirements of Caenorhabditis
978 elegans. *Genes Nutr* **14**, 15 (2019).
979 32. Okabe, Y. & Medzhitov, R. Tissue biology perspective on macrophages. *Nat Immunol* **17**,
980 9-17 (2016).
981 33. Glass, C.K. & Natoli, G. Molecular control of activation and priming in macrophages. *Nat*
982 *Immunol* **17**, 26-33 (2016).
983 34. Kopf, M., Schneider, C. & Nobs, S.P. The development and function of lung-resident
984 macrophages and dendritic cells. *Nat Immunol* **16**, 36-44 (2015).
985 35. Anthony, R.M., Rutitzky, L.I., Urban, J.F., Jr., Stadecker, M.J. & Gause, W.C. Protective
986 immune mechanisms in helminth infection. *Nat Rev Immunol* **7**, 975-987 (2007).
987 36. Chen, F., *et al.* B Cells Produce the Tissue-Protective Protein RELMalpha during Helminth
988 Infection, which Inhibits IL-17 Expression and Limits Emphysema. *Cell Rep* **25**, 2775-2783
989 e2773 (2018).
990 37. Marsland, B.J., Kurrer, M., Reissmann, R., Harris, N.L. & Kopf, M. Nippostrongylus
991 brasiliensis infection leads to the development of emphysema associated with the
992 induction of alternatively activated macrophages. *Eur J Immunol* **38**, 479-488 (2008).
993 38. Roquilly, A., *et al.* Alveolar macrophages are epigenetically altered after inflammation,
994 leading to long-term lung immunoparalysis. *Nat Immunol* **21**, 636-648 (2020).

995 39. Potian, J.A.*, et al.* Preexisting helminth infection induces inhibition of innate pulmonary
996 anti-tuberculosis defense by engaging the IL-4 receptor pathway. *J Exp Med* **208**, 1863-
997 1874 (2011).
998 40. Yamaguchi, R.*, et al.* Mechanism of interleukin-13 production by granulocyte-
999 macrophage colony-stimulating factor-dependent macrophages via protease-activated
1000 receptor-2. *Blood Cells Mol Dis* **55**, 21-26 (2015).
1001 41. Minutti, C.M.*, et al.* Local amplifiers of IL-4Ralpha-mediated macrophage activation
1002 promote repair in lung and liver. *Science* **356**, 1076-1080 (2017).
1003 42. Espinosa, V.*, et al.* Type III interferon is a critical regulator of innate antifungal immunity.
1004 *Sci Immunol* **2**(2017).
1005 43. Barron, L.*, et al.* Role of arginase 1 from myeloid cells in th2-dominated lung
1006 inflammation. *PloS one* **8**, e61961 (2013).
1007 44. Ewels, P.A.*, et al.* The nf-core framework for community-curated bioinformatics
1008 pipelines. *Nature biotechnology* **38**, 276-278 (2020).
1009 45. Liao, Y., Smyth, G.K. & Shi, W. featureCounts: an efficient general purpose program for
1010 assigning sequence reads to genomic features. *Bioinformatics* **30**, 923-930 (2014).
1011 46. Pertea, M.*, et al.* StringTie enables improved reconstruction of a transcriptome from
1012 RNA-seq reads. *Nature biotechnology* **33**, 290-295 (2015).
1013 47. Dobin, A.*, et al.* STAR: ultrafast universal RNA-seq aligner. *Bioinformatics* **29**, 15-21
1014 (2013).
1015 48. Love, M.I., Huber, W. & Anders, S. Moderated estimation of fold change and dispersion
1016 for RNA-seq data with DESeq2. *Genome biology* **15**, 550 (2014).
1017 49. Weinstein, J.S.*, et al.* Correction: STAT4 and T-bet control follicular helper T cell
1018 development in viral infections. *J Exp Med* **215**, 999 (2018).
1019

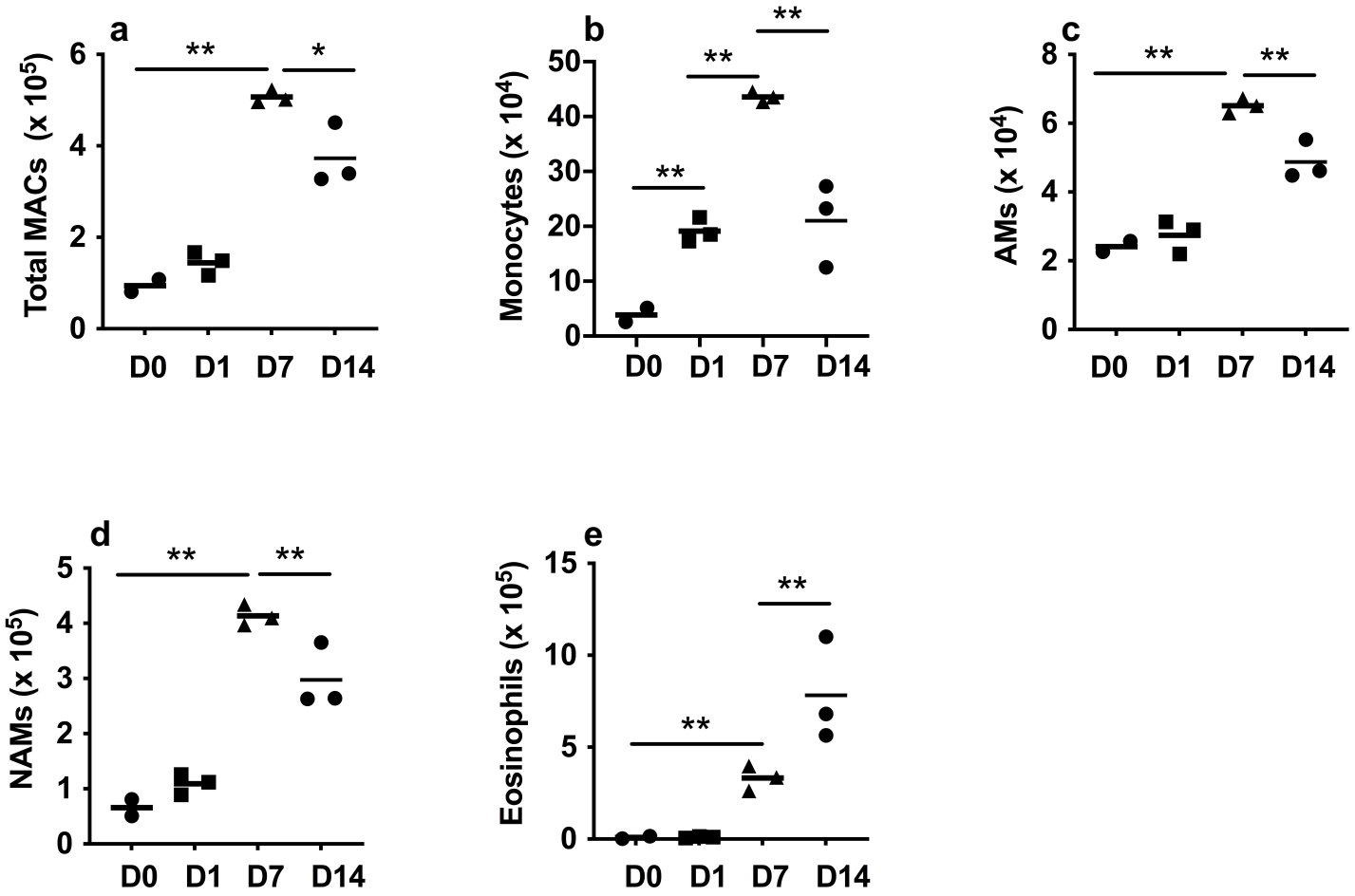
a
Total MACs (x 10^5)
0
2
4
6
**
*
D0
D1
D7
D14
b
Monocytes (x 10^4)
0
10
20
30
40
50
**
**
**
D0
D1
D7
D14
c
AMs (x 10^4)
0
2
4
6
8
**
**
D0
D1
D7
D14
d
NAMs (x 10^5)
0
1
2
3
4
5
**
**
D0
D1
D7
D14
e
Eosinophils (x 10^5)
0
5
10
15
**
**
D0
D1
D7
D14

Fig. 1

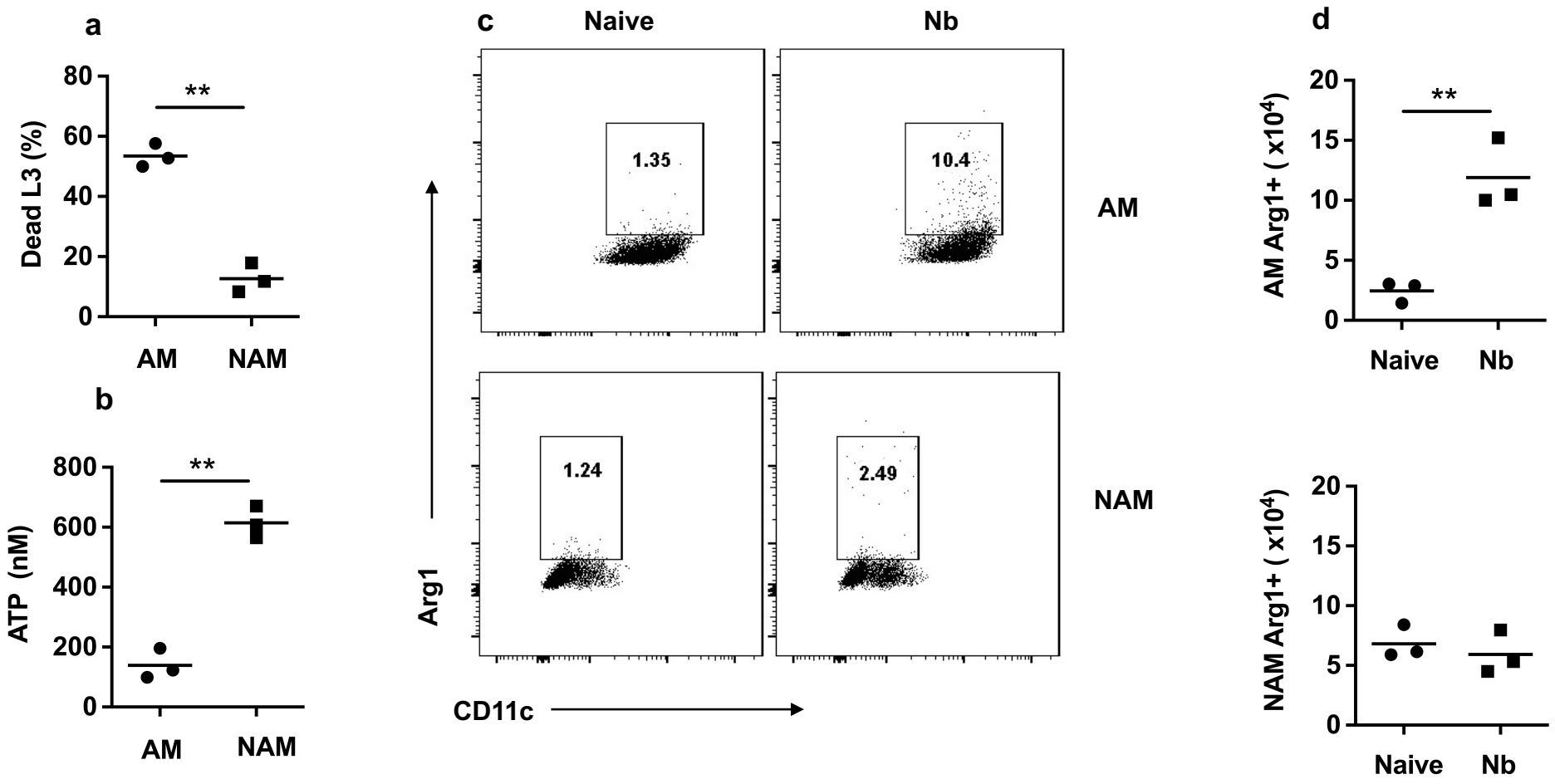
a
Dead L3 (%)
80
60
40
20
0
**
AM
NAM
b
ATP (nM)
800
600
400
200
0
**
AM
NAM
c
Naive
Nb
1.35
10.4
AM
1.24
2.49
NAM
Arg1
CD11c
d
AM Arg1+ ( x10^4)
20
15
10
5
0
**
Naive
Nb
NAM Arg1+ ( x10^4)
20
15
10
5
0
Naive
Nb

Fig. 2

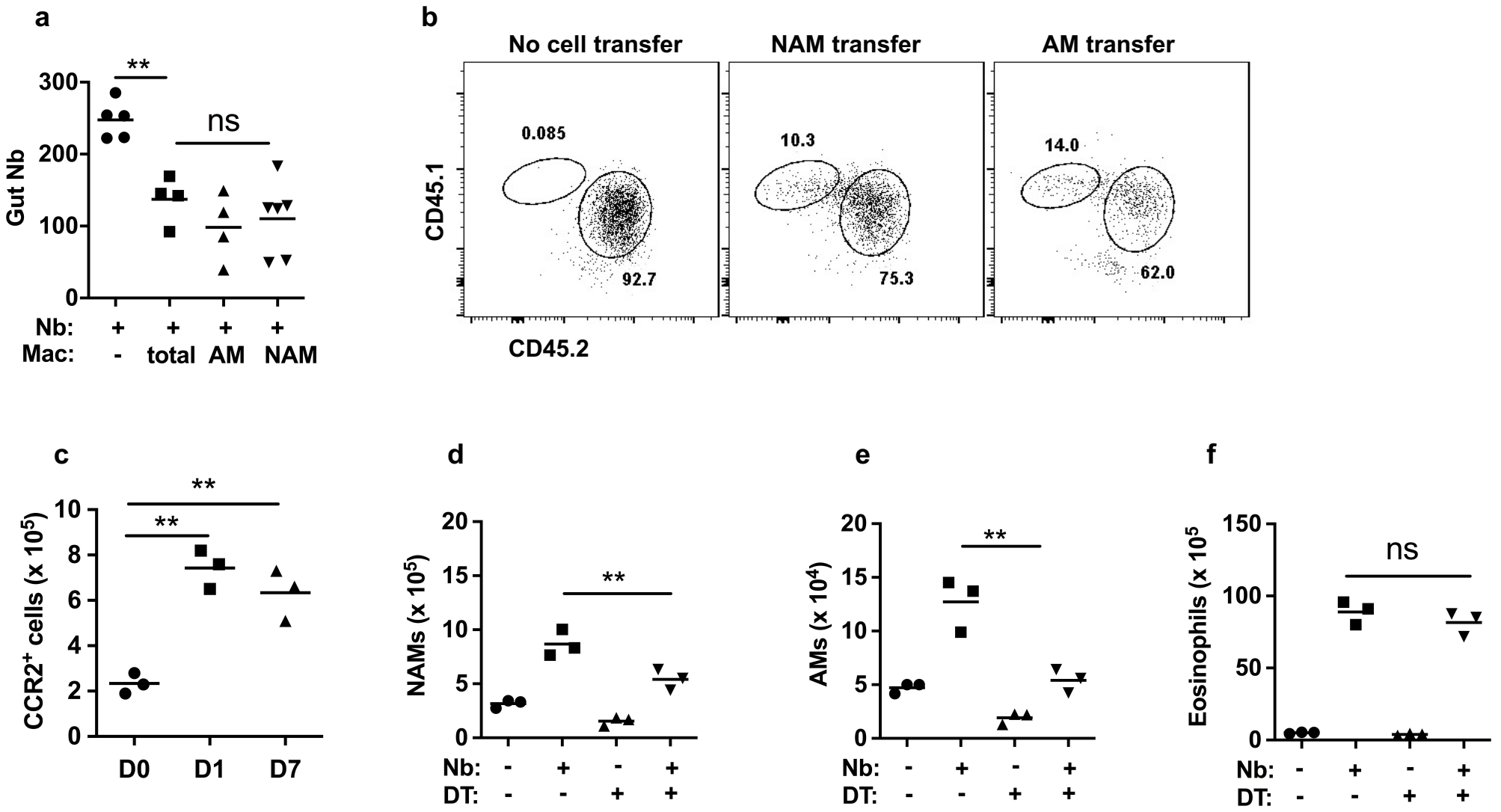
a
Gut Nb
300
200
100
0
**
ns
Nb: + + + +
Mac: - total AM NAM
b
No cell transfer
NAM transfer
AM transfer
CD45.1
CD45.2
0.085
92.7
10.3
75.3
14.0
62.0
c
CCR2+ cells (x 10^5)
10
8
6
4
2
0
**
**
D0
D1
D7
d
NAMs (x 10^5)
20
15
10
5
0
**
Nb: - + - +
DT: - - + +
e
AMs (x 10^4)
20
15
10
5
0
**
Nb: - + - +
DT: - - + +
f
Eosinophils (x 10^5)
150
100
50
0
ns
Nb: - + - +
DT: - - + +

Fig. 3

Fig. 4

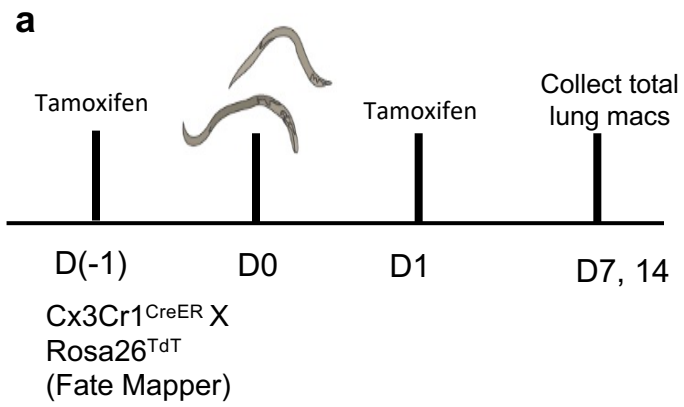
a
Tamoxifen
Tamoxifen
Collect total lung macs
D(-1)
D0
D1
D7, 14
Cx3Cr1CreER X
Rosa26TdT
(Fate Mapper)

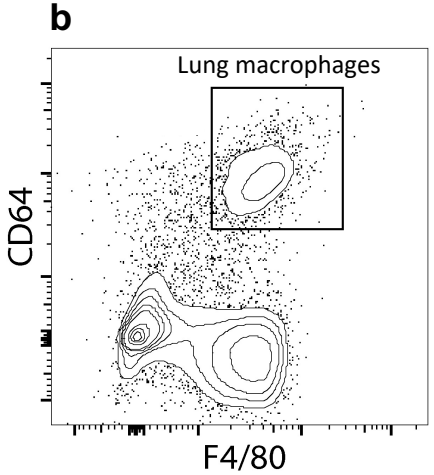
b
Lung macrophages
CD64
F4/80

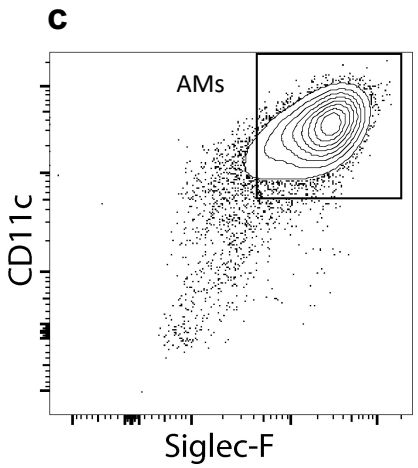
c
AMs
CD11c
Siglec-F

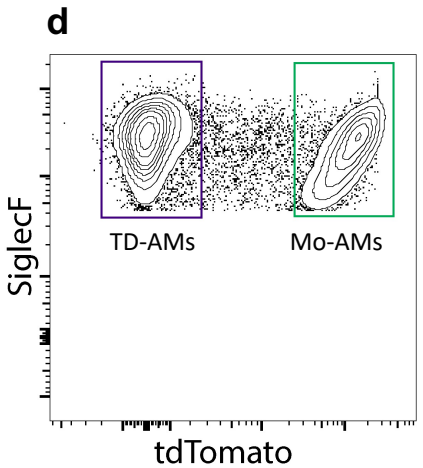
d
SiglecF
TD-AMs
Mo-AMs
tdTomato

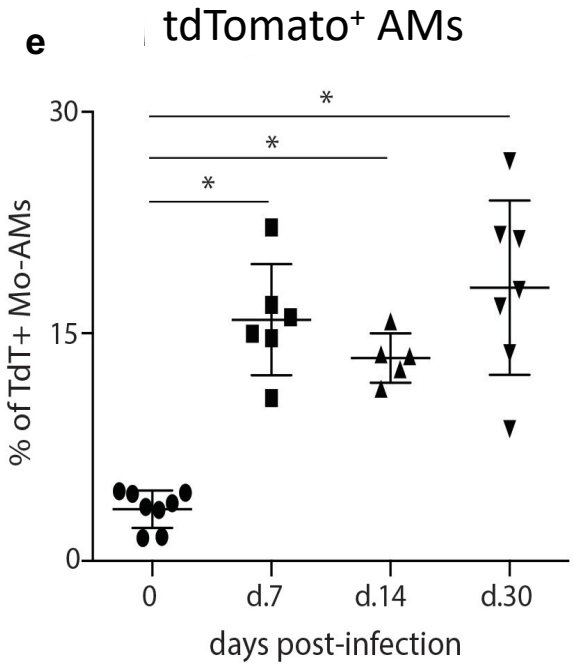
e
tdTomato+ AMs
% of TdT+ Mo-AMs
30
15
0
*
*
*
0
d.7
d.14
d.30
days post-infection

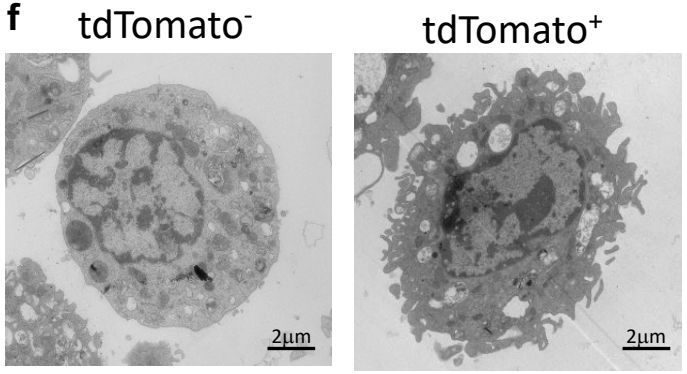
f
tdTomato-
tdTomato+
2µm
2µm

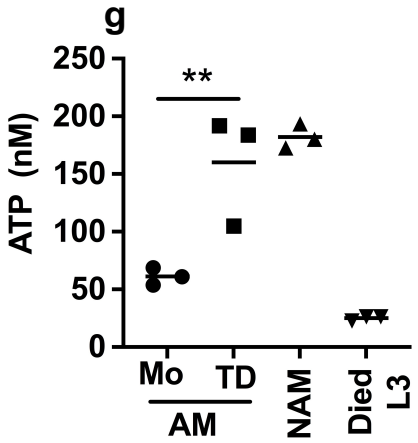
g
ATP (nM)
250
200
150
100
50
0
**
Mo
TD
AM
NAM
Died L3

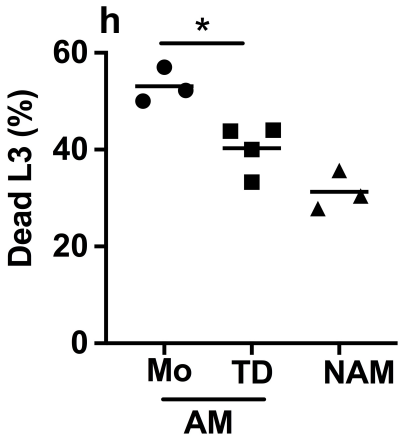
h
Dead L3 (%)
60
40
20
0
*
Mo
TD
AM
NAM

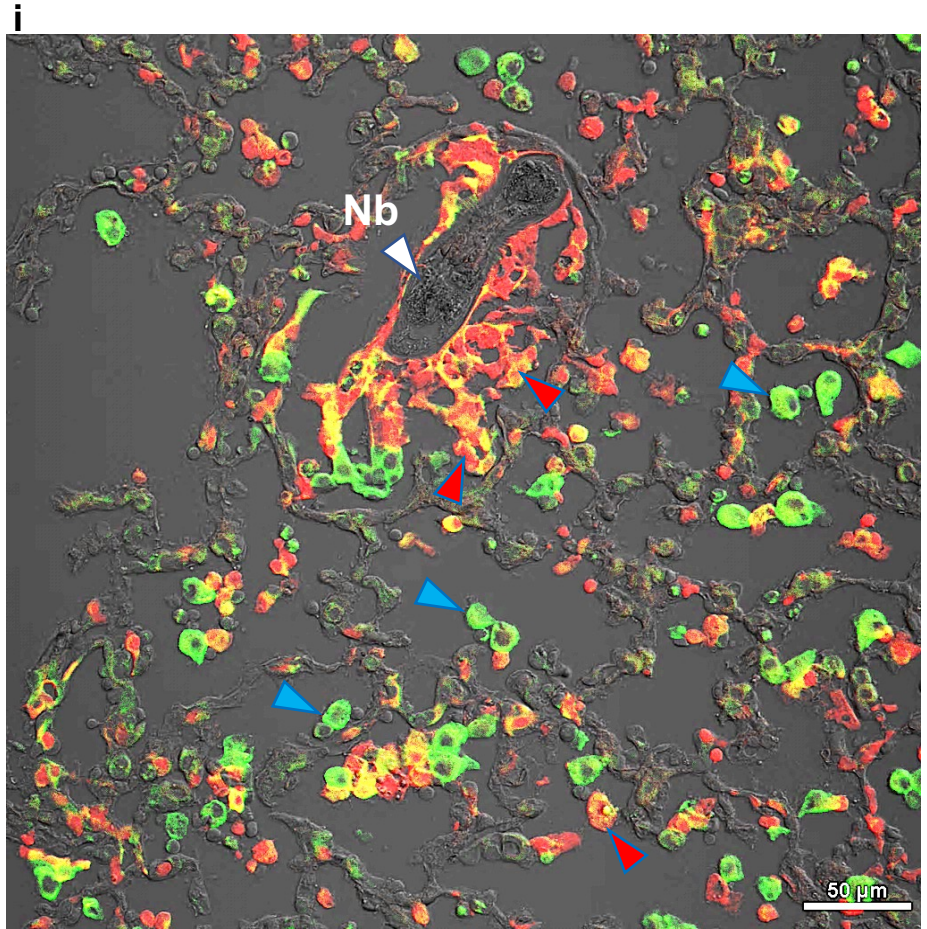
i
Nb
50 µm

Supplementary Fig. 1

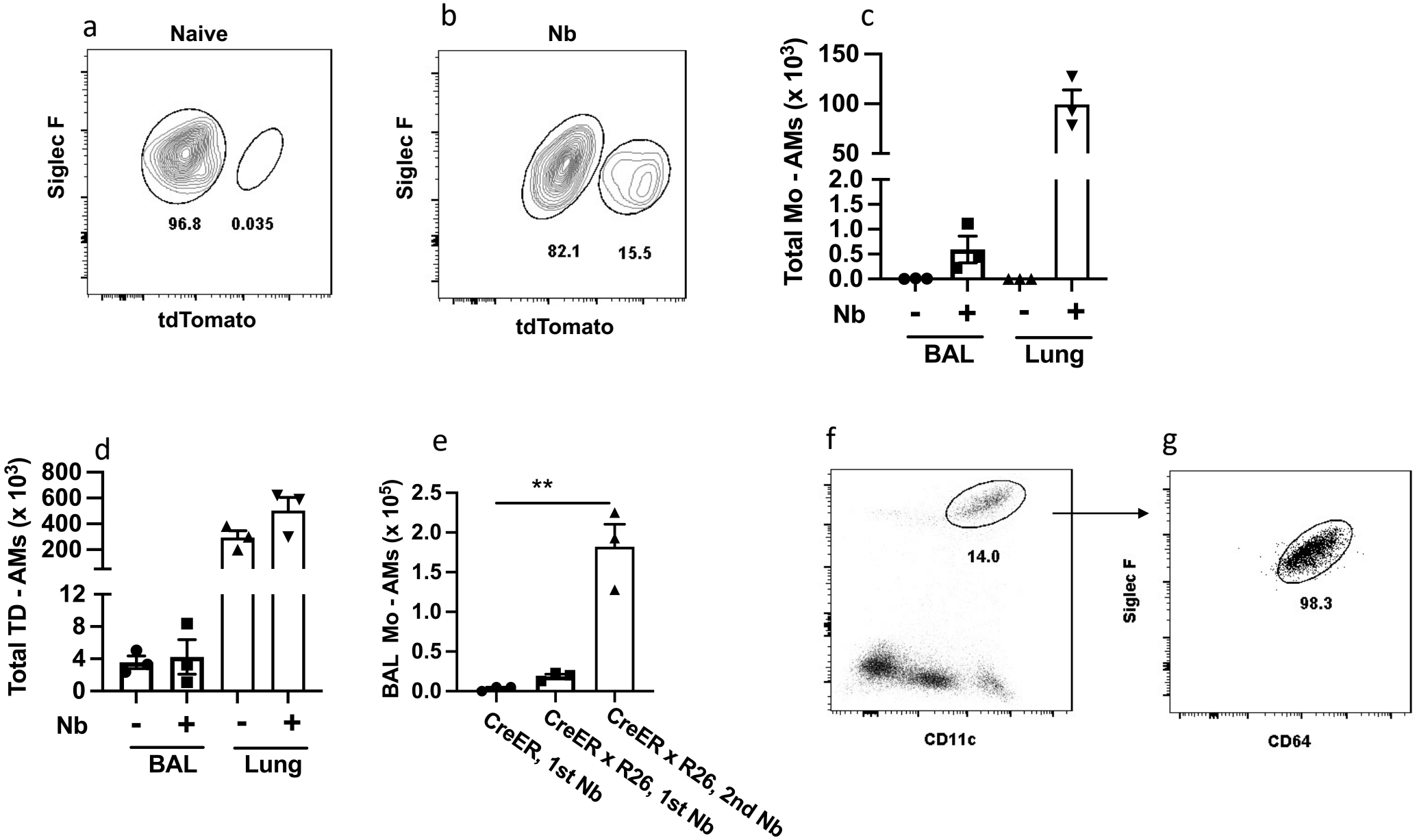

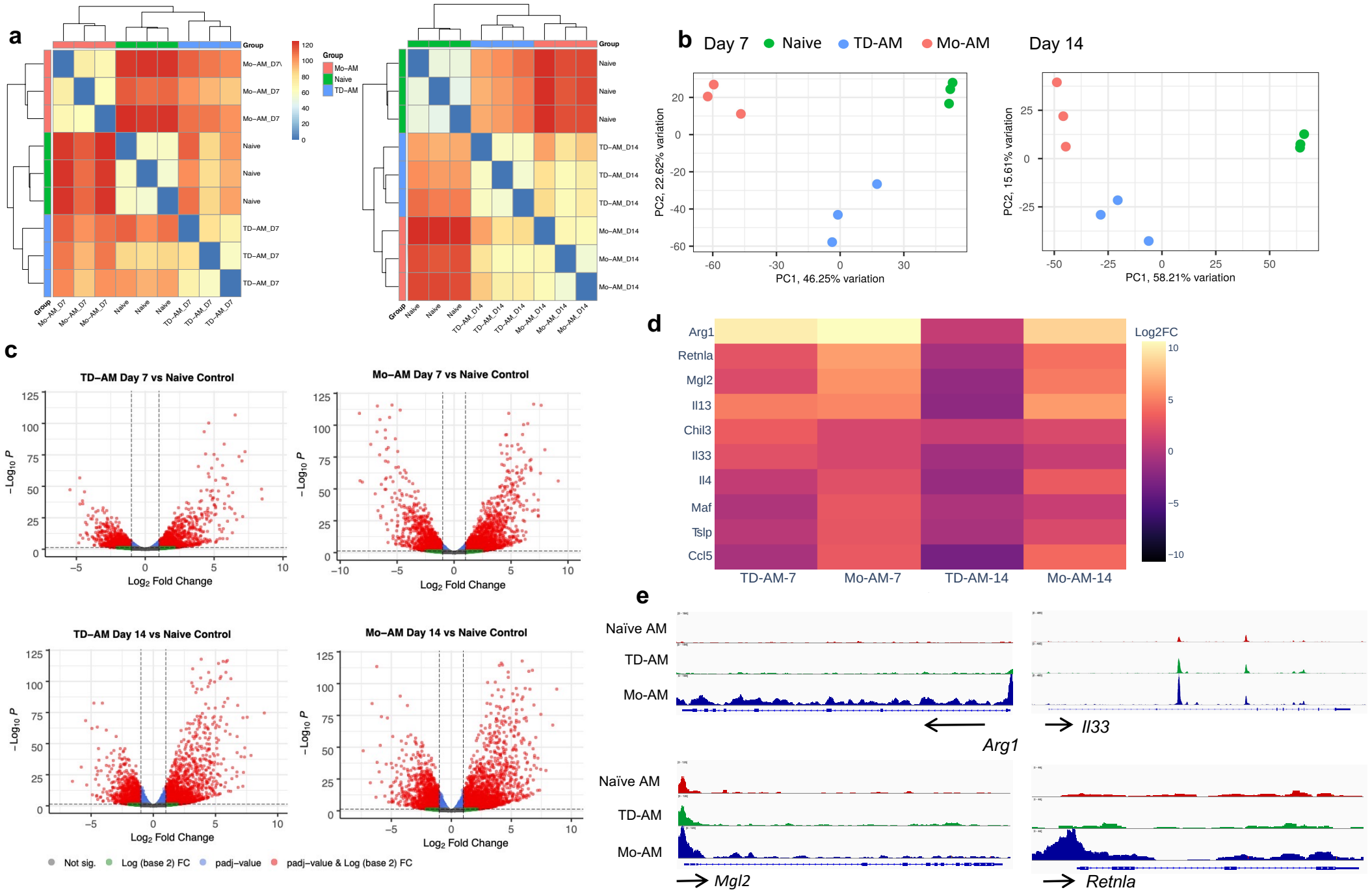
a
Group
Mo–AM
Naive
TD–AM
Mo–AM_D7
Naive
TD–AM_D7
TD–AM_D14
Mo–AM_D14
b
Day 7
Naive
TD-AM
Mo-AM
Day 14
PC2, 22.62% variation
PC1, 46.25% variation
PC2, 15.61% variation
PC1, 58.21% variation
c
TD–AM Day 7 vs Naive Control
Mo–AM Day 7 vs Naive Control
TD–AM Day 14 vs Naive Control
Mo–AM Day 14 vs Naive Control
−Log10 P
Log2 Fold Change
Not sig.
Log (base 2) FC
padj–value
padj–value & Log (base 2) FC
d
Arg1
Retnla
Mgl2
Il13
Chil3
Il33
Il4
Maf
Tslp
Ccl5
TD-AM-7
Mo-AM-7
TD-AM-14
Mo-AM-14
Log2FC
e
Naïve AM
TD-AM
Mo-AM
Arg1
Il33
Mgl2
Retnla

Fig. 5

a

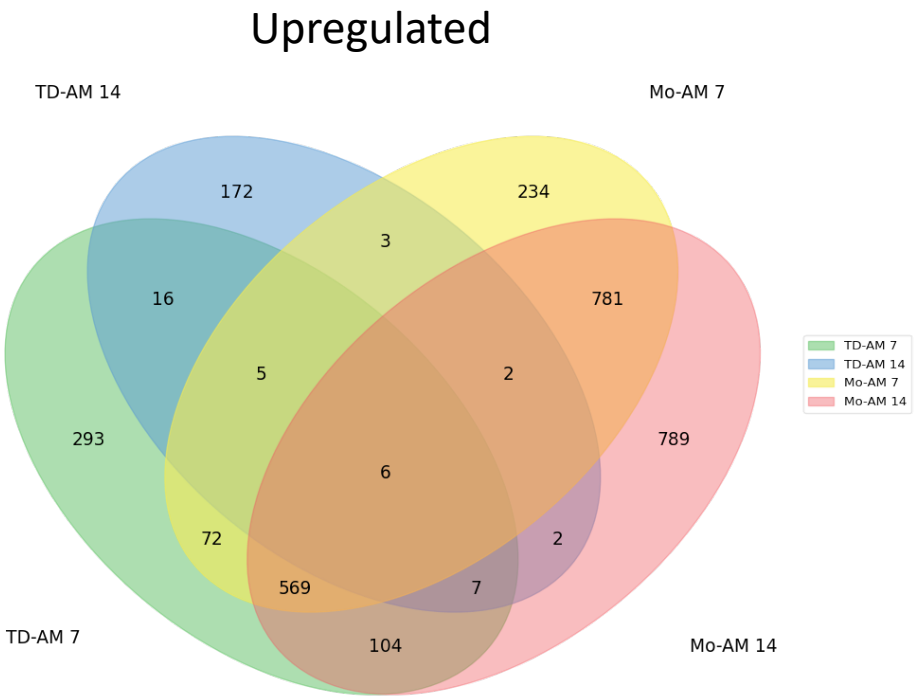


b

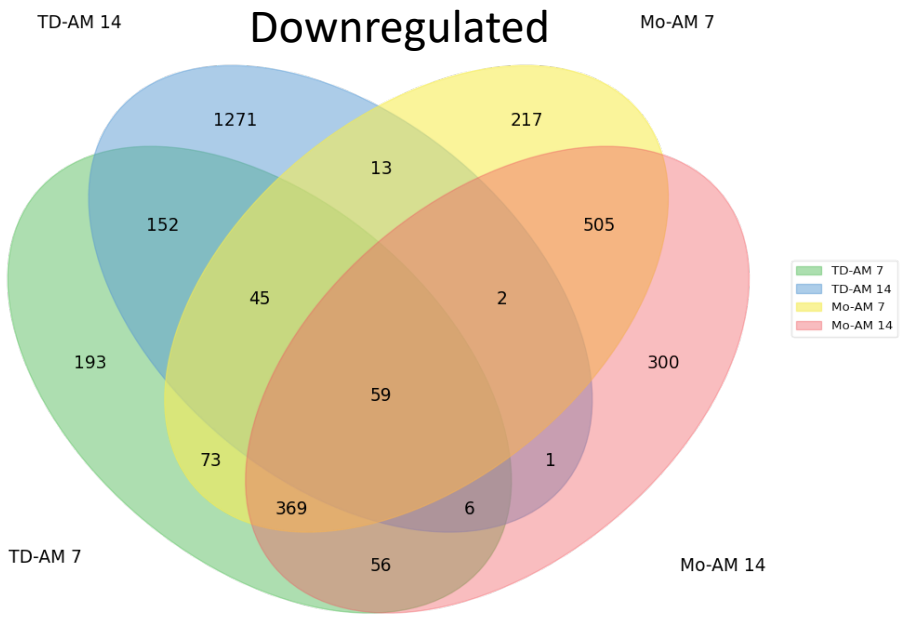


c

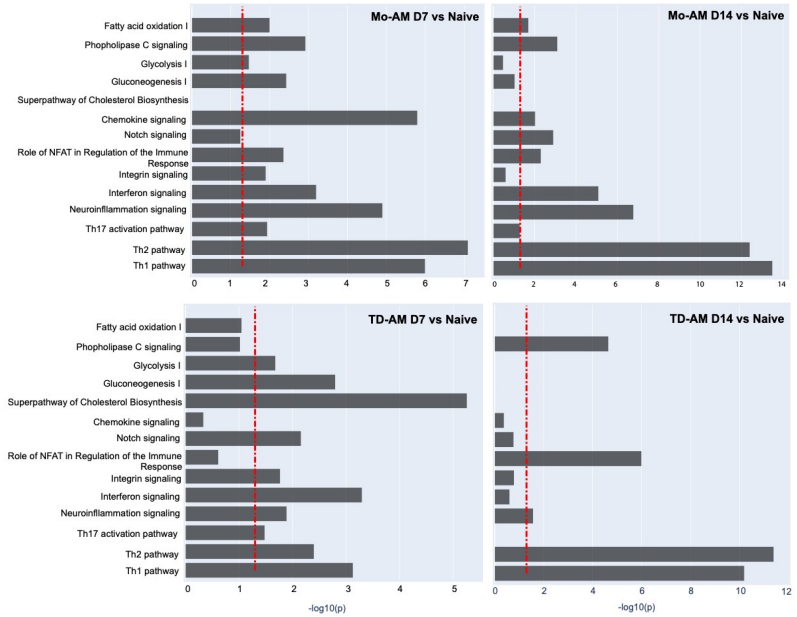


d

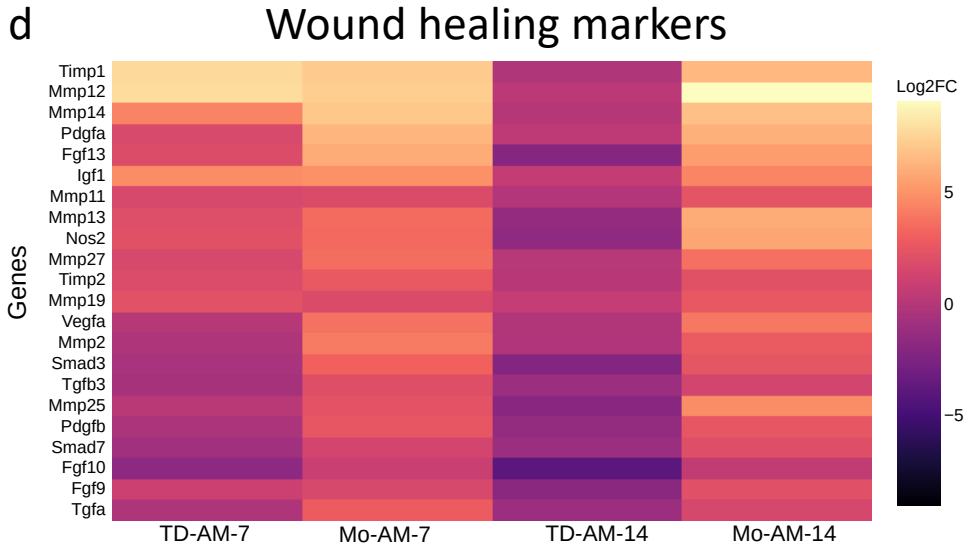


Supplementary Fig. 2

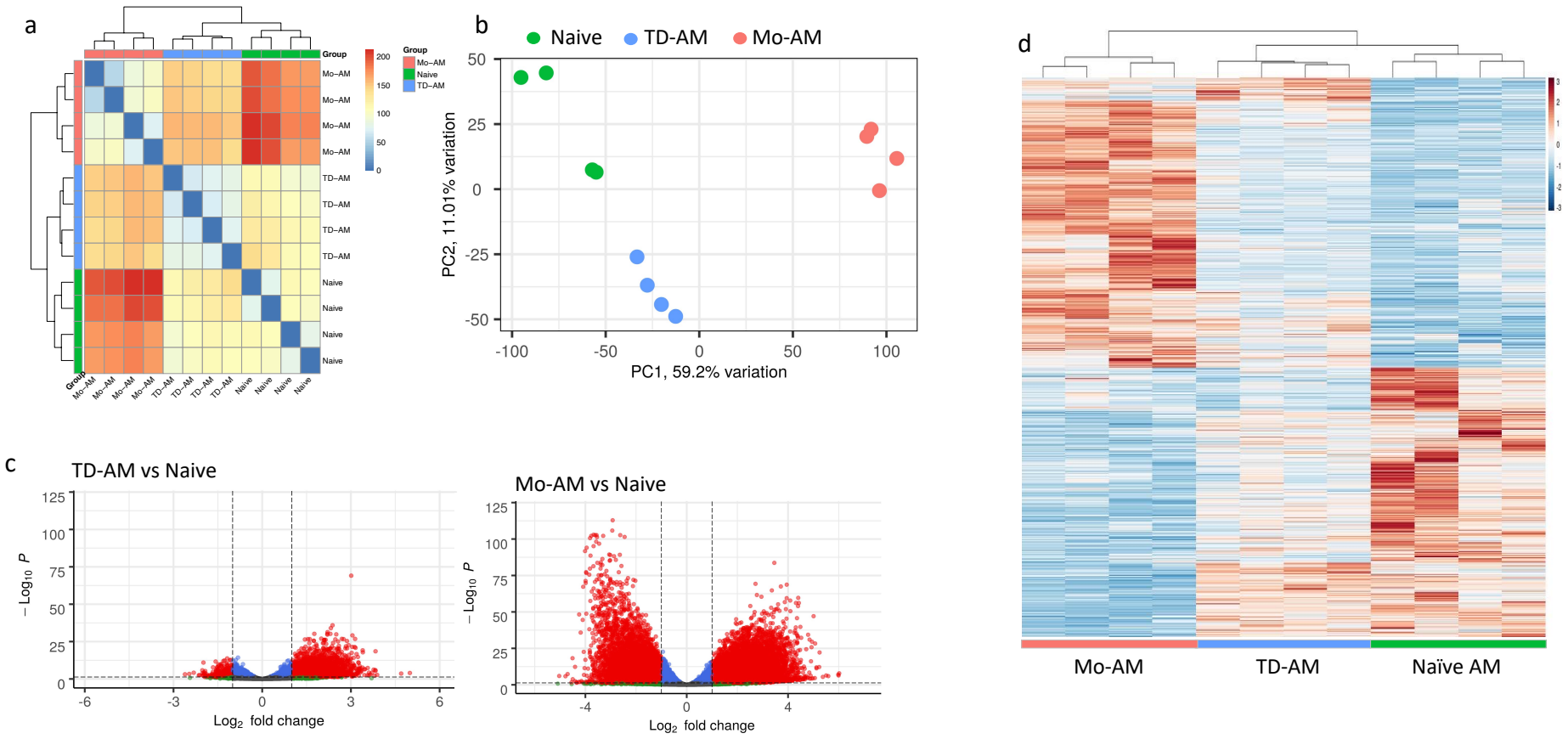


Supplementary Fig. 3

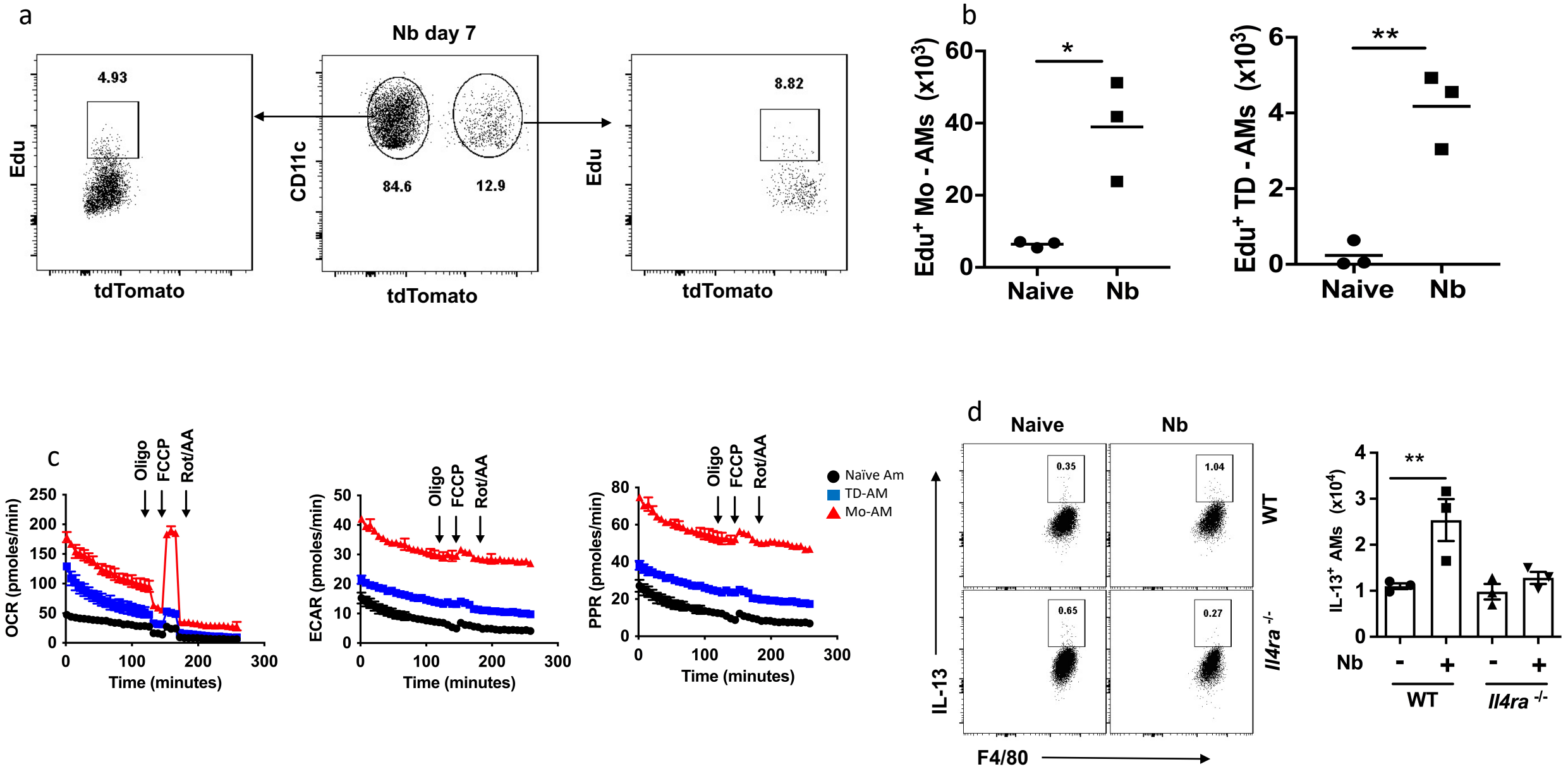


Supplementary Fig. 4

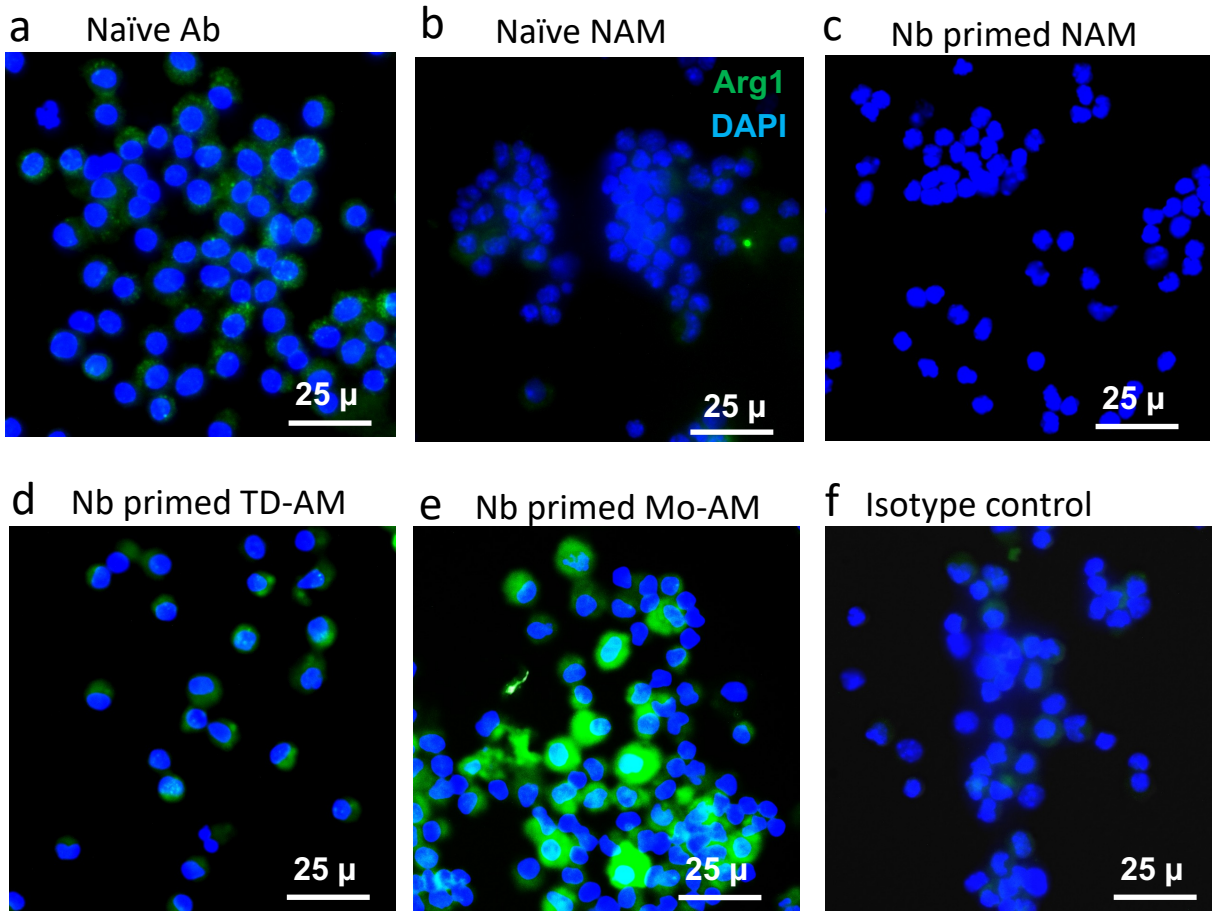


Supplementary Fig. 5

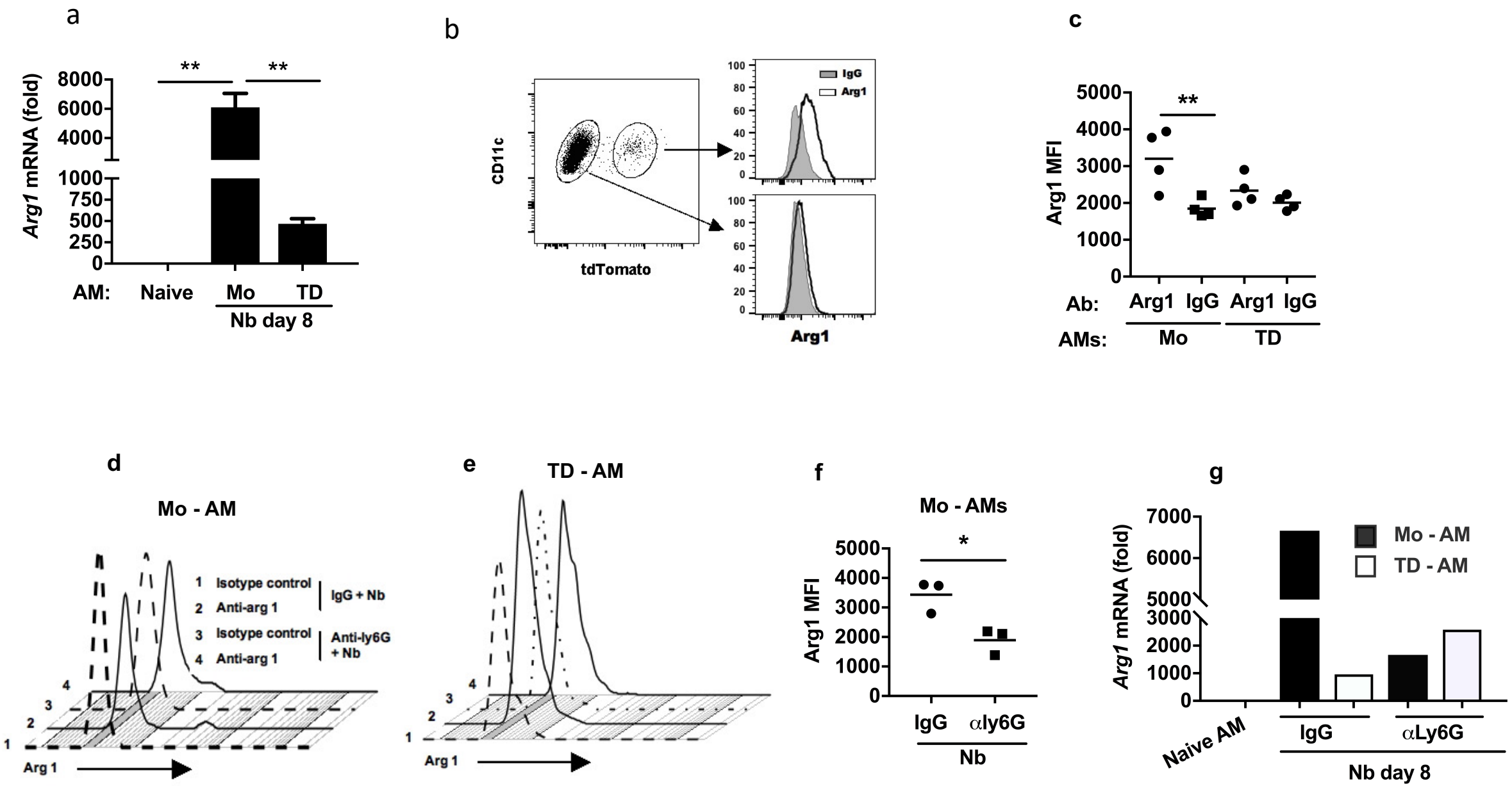
a
Arg1 mRNA (fold)
8000
6000
4000
1000
750
500
250
0
**
**
AM:
Naive
Mo
TD
Nb day 8
b
CD11c
tdTomato
IgG
Arg1
Arg1
c
Arg1 MFI
5000
4000
3000
2000
1000
0
**
Ab:
Arg1
IgG
Arg1
IgG
AMs:
Mo
TD
d
Mo - AM
1 Isotype control
2 Anti-arg 1
IgG + Nb
3 Isotype control
4 Anti-arg 1
Anti-ly6G + Nb
Arg 1
e
TD - AM
Arg 1
f
Mo - AMs
Arg1 MFI
5000
4000
3000
2000
1000
0
*
IgG
αly6G
Nb
g
Arg1 mRNA (fold)
7000
6000
5000
3000
2000
1000
0
Mo - AM
TD - AM
Naive AM
IgG
αLy6G
Nb day 8

Fig. 6

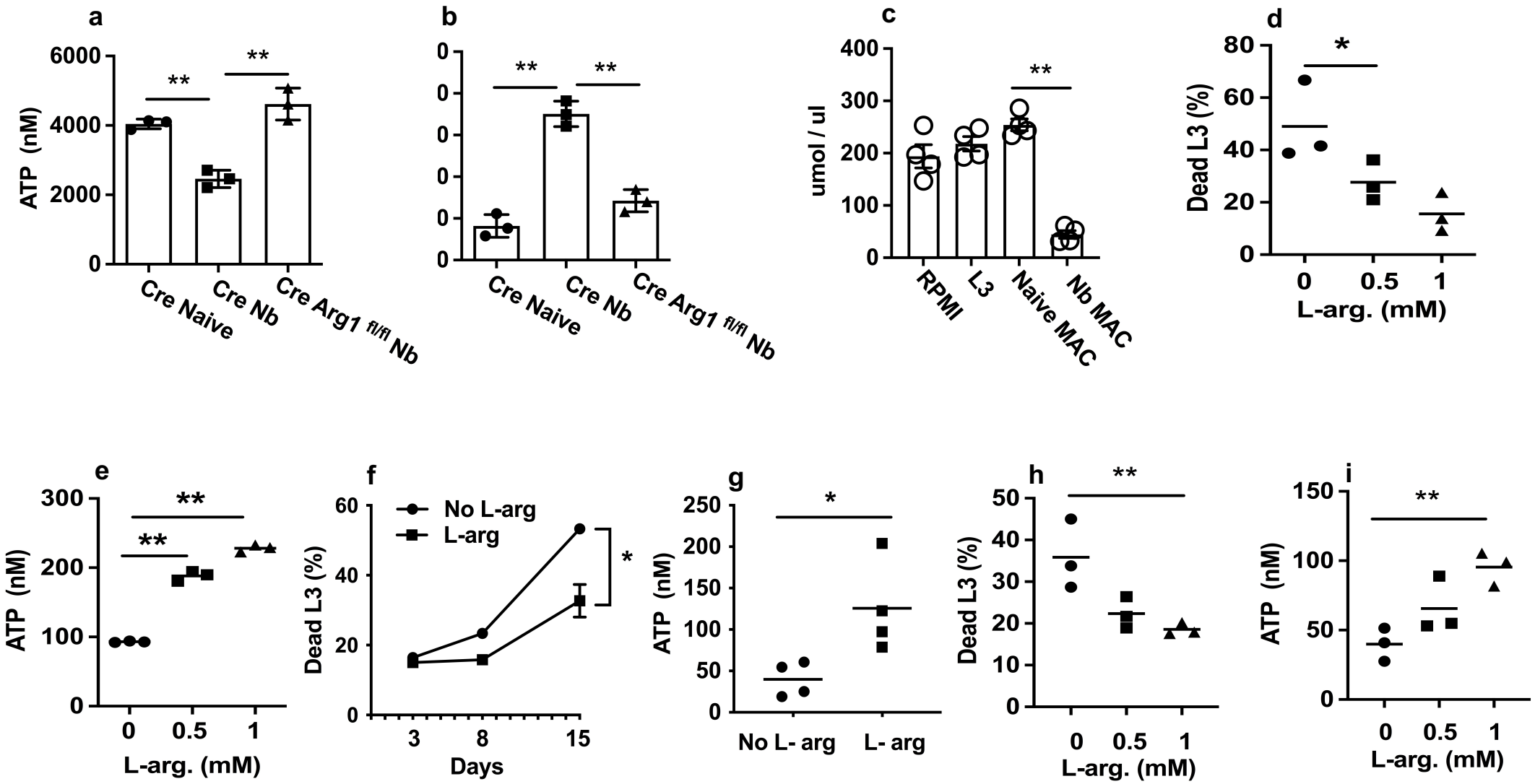
a
ATP (nM)
6000
4000
2000
0
**
**
Cre Naive
Cre Nb
Cre Arg1 fl/fl Nb
b
**
**
Cre Naive
Cre Nb
Cre Arg1 fl/fl Nb
c
umol / ul
400
300
200
100
0
**
RPMI
L3
Naive MAC
Nb MAC
d
Dead L3 (%)
80
60
40
20
0
*
0
0.5
1
L-arg. (mM)
e
ATP (nM)
300
200
100
0
**
**
0
0.5
1
L-arg. (mM)
f
Dead L3 (%)
60
40
20
0
No L-arg
L-arg
*
3
8
15
Days
g
ATP (nM)
250
200
150
100
50
0
*
No L- arg
L- arg
h
Dead L3 (%)
50
40
30
20
10
0
**
0
0.5
1
L-arg. (mM)
i
ATP (nM)
150
100
50
0
**
0
0.5
1
L-arg. (mM)

Fig. 7